Functionally distinct mutations within AcrB underpin antibiotic resistance in different lifestyles

Eleftheria Trampari[1], Filippo Prischi[2], Attilio V. Vargiu[3], Justin Abi-Assaf[1], Vassiliy N. Bavro[2*], Mark A Webber[1,4*]

Affiliations:

[1]Quadram Institute Bioscience, Norwich Research Park, Norwich, Norfolk, NR4 7UQ, U.K.

[2]School of Life Sciences, University of Essex, Wivenhoe Park, Colchester, CO4 3SQ, U.K.

[3]Department of Physics, University of Cagliari, S. P. 8, km. 0.700, 09042, Monserrato, Italy

[4]Medical School, University of East Anglia, Norwich Research Park, Norwich, Norfolk, NR4 7UA, U.K.

*v.bavro@essex.ac.uk

*mark.webber@quadram.ac.uk

Key words:

Efflux, macrolides, cephalosporins, biofilm, evolution, *Salmonella*

Abstract

Antibiotic resistance is a pressing healthcare challenge and is mediated by various mechanisms including active export of drugs *via* multidrug efflux systems which prevent drug accumulation within the cell. Here, we studied how *Salmonella* evolved resistance to two key antibiotics, cefotaxime and azithromycin, when grown planktonically, or as a biofilm. Resistance to both drugs emerged in both conditions and was associated with different substitutions within the efflux-associated transporter, AcrB. Azithromycin exposure selected for an R717L substitution, while cefotaxime for Q176K. Additional mutations in *ramR* or *envZ*, accumulated concurrently with the R717L or Q176K substitutions respectively, resulting in clinical resistance to the selective antibiotics and cross-resistance to other drugs. Structural, genetic, and phenotypic analysis showed the two AcrB substitutions confer their benefits in profoundly different ways. R717L reduces steric barriers associated with transit through the substrate channel 2 of AcrB. Q176K increases binding energy for cefotaxime, improving recognition in the distal binding pocket, resulting in increased efflux efficiency. Finally, we show the R717 substitution is present in isolates recovered around the world.

Introduction

Antibiotics are crucial for modern medicine, but their introduction and use has resulted in the widespread emergence of antibiotic resistant bacteria. Bacteria can rapidly adapt to changing environments and exposure to antibiotics selects for genetic traits that confer resistance, promoting expansion of resistant mutants [1]. Several important mechanisms of antibiotic resistance have been described including enzymatic degradation, target modification or bypass, membrane alterations and changes in efflux activity [2].

Energy-dependent efflux systems are responsible for the export of toxic compounds from the cell to the environment, are found in all bacteria, and act synergistically with other mechanisms of resistance [3]. In Gram-negative bacteria, efflux systems are tripartite transmembrane protein complexes that secrete molecules from the periplasm to the exterior of the cell. The 'Resistance Nodulation cell Division' (RND) efflux family is the most important for antibiotic export [4-7] and RND systems have been shown to determine the basal level of susceptibility of cells to many antimicrobials.

Within the RND family the Enterobacterial AcrAB-TolC is the best characterised tripartite efflux system and is built around the energised inner membrane H^+/drug-antiporter AcrB [5]. The functional unit of AcrB is a homotrimer, containing three functionally interdependent protomers, cycling consecutively through loose (L), tight (T) and open (O) conformational states during the efflux cycle, in a supposedly cooperative fashion [8,9]. This allosteric "pumping" allows a drug to be acquired from either periplasmic space or the outer leaflet of the inner membrane and passed out of the cell via a conduit produced by the partner outer membrane factor (OMF) and periplasmic adaptor proteins (PAPs) [4,10,11].

AcrB can export multiple classes of antibiotics including macrolides, β-lactams, quinolones, rifamycins, tetracyclines, as well as other substrates including anticancer drugs, bile salts, dyes and solvents [12-17]. This broad substrate specificity is underpinned by the presence of distinct binding pockets within the pump. Drugs of different molecular weight are suggested to be processed in two principal multisite binding pockets, termed the 'Proximal Binding Pocket' (PBP) and the 'Distal Binding Pocket' (DBP), which have wide specificities and are separated from each other by the so-called gating or switch-loop [8,18-21]. High molecular weight drugs appear to be

predominantly recognised by the PBP, and recent evidence suggests they may be exported directly to the OMF, bypassing the DBP altogether [22], whilst low-molecular weight drugs are thought to be processed predominantly within the DBP [8,19]. Access to these multisite binding pockets is governed by at least four distinct substrate channels, each of which also exhibit different substrate specificities [22-26]. The principal periplasmic drug access channel for polar compounds is proposed to be channel 2 (CH2), preferred by macrolide, rifamycin and tetracycline antibiotics [23,26], while hydrophobic compounds, such as linezolid, phenicols, fluoroquinolones and novobiocin are suggested to be acquired from the outer leaflet of the inner membrane via channel 1 (CH1). Compounds entering via CH1 and CH2 are thought to pass sequentially through both the PBP and DBP, with access to the latter being restricted by the switch-loop. On the other hand, channel 3 (CH3), implicated in the transport of planar aromatic cations (PACs), such as benzalkonium chloride, crystal violet, ethidium bromide, methylene blue, and rhodamine 6G, is suggested to bypass the PBP and the gating loop altogether, allowing direct access to the DBP [26]. Similarly, membrane-localized carboxylated substrates, such as fusidic acid and hydrophobic β-lactams, access the pump via a groove between the transmembrane helices TM1 and TM2, which forms part of the recently described CH4, again bypassing the PBP, allowing direct access to the DBP [25].

Whilst AcrB helps determine the intrinsic level of susceptibility to many drugs it can also confer resistance when over-expressed due to mutations in the regulatory circuits controlling its production [27,28]. Changes within AcrB itself that alter export of specific antibiotics can also be selected by antibiotic exposure [6,29-33]. For example substitutions M78I and P319L were shown to confer decreased susceptibility to multiple antimicrobial substrates [34] and substitution G288D has been linked to increased tolerance against ciprofloxacin [30]. These examples demonstrate how selection can favour strains with mutant AcrB proteins altering substrate recognition or export efficiency, as well as mutations in regulators which control pump expression.

Despite the benefits provided, the selection of resistance can have impacts on fitness for a bacterium, and the fate of any resistance mutation that occurs within a population will depend on how permissive it is for the organism's lifestyle [35]. Efflux pumps contribute to various important cellular functions including those relevant to

infection. Relationships between efflux pump function and the ability to form biofilms has been established in multiple species [36] and loss of pump function commonly compromises virulence [37]. Life within a biofilm is common for bacteria and is an important determinant of many infections, as biofilms are also by nature highly tolerant of antibiotics [38].

In this work we used an evolution model to study how subinhibitory concentrations of two clinically important antibiotics, cefotaxime (Cef) and azithromycin (Azi), representing two major structural classes of antibiotics, cephalosporins and macrolides respectively, selected for resistance mechanisms in *Salmonella*, in both biofilm and planktonic conditions. We found that both antibiotics selected for unique substitutions within AcrB. We confirmed these substitutions affect antibiotic susceptibility and identified their prevalence in the real world of these mutant *acrB* alleles. Using structural and computational approaches, supported by genetic and phenotypic analysis, we demonstrate how these two distinct substitutions within AcrB facilitate drug translocation through the efflux conduit of the pump in fundamentally different ways.

Results

Cefotaxime and azithromycin both select for substitutions within AcrB

To investigate adaptation of *Salmonella* to clinically important antibiotics, we used representatives of two antibiotic families amongst the drugs of choice for treatment of Salmonellosis: cefotaxime, a 3rd generation cephalosporin and azithromycin, a 2nd generation macrolide. We repeatedly exposed independent planktonic and biofilm lineages of *S.* Typhimurium 14028S to concentrations of azithromycin and cefotaxime that restricted planktonic growth rates by approximately 50% (10 and 0.062 μg/ mL, respectively) for 17 passage cycles (each lasting 72 hours). Estimation of the number of generations each population went through (based on calculating log2 x the dilution factor of cells in each condition by the number of passages) gave ~170 for planktonic conditions, ~264 for cefotaxime-exposed biofilms, ~289 for azithromycin-exposed biofilms and ~317 for control biofilms. The number of generations was higher for biofilms than planktonic conditions as we used a bead-based evolution model [39], where the dilution factor of cells which occurs when new, sterile beads are colonised, is higher than the dilution in planktonic cultures.

Phenotyping of isolates recovered over time from the experiments found that both antibiotics rapidly selected for resistance (**Supplementary Figure 1**). Genome sequencing identified drug-specific mutations resulting in substitutions within AcrB. Cefotaxime selected for a Q176K substitution and azithromycin for a R717L substitution. To define the phenotypic impacts of these mutations in more detail and to determine when they emerged in each experiment, three single colonies were recovered from each of three time points (early, middle, and late; corresponding to passages 1, 9 and 17 respectively). Isolation of single isolates was carried out for each of the four independent exposed biofilm lineages, as well as the exposed planktonic and unexposed biofilm control (20 isolates in total, derived from exposed conditions). These mutants were then phenotyped and genome sequenced.

Exposure to azithromycin rapidly selected for the R717L mutation within AcrB after just a single exposure under stress in all populations regardless of the selective context (biofilm or planktonic). The R717L mutation was associated with an 8-fold increase in the MIC for azithromycin. **Figure 1a** shows this substitution was present in all isolates over time from one randomly selected biofilm lineage (as well as being

in all the populations sequenced). An additional mutation within the local transcriptional repressor *ramR* controlling the expression of the *acrAB* multidrug operon [40] (corresponding to a T18P substitution), emerged after passage 9 in addition to the *acrB* mutation. This was associated with a further increase in MIC of azithromycin to 32-fold higher relative to the parent strain. This mutation was also linked with increased MICs of different classes of antibiotics, including chloramphenicol (8-fold increase) and ciprofloxacin (8-fold change) consistent with previous work [41]. No other additional mutations were identified in the isolated mutants, and none were seen to repeatedly occur in multiple populations.

The dynamics of selection for substitutions within AcrB by cefotaxime were different. Initial populations obtained a mutation within *envZ* (R397H) leading to reduced permeability to cefotaxime (which we have recently described in detail, [42]). In contrast to the azithromycin exposure where the *acrB* mutation emerged first, the Q176K substitution within AcrB emerged half-way through the experiment (passage 9) and was always seen in conjunction with the *envZ* mutation. Notably, Q176K was only recovered from planktonic populations. The acquisition of these two mutations was associated with an MIC increase for cefotaxime to the clinical breakpoint (2 µg/ mL), compared to the parent strain's MIC (0,125 µg/ mL) (**Figure 1b**). Increased tolerance was maintained throughout the course of the experiment for mutants carrying both substitutions. In passage 17, the measured susceptibility of these strains was a fold lower compared to passage 9. This is not considered significant and is accepted as error of the method. Fitness, in the form of bacterial growth in liquid culture, of isolates carrying the two identified substitutions, was not affected, as measured by growth curve assays (**Supplementary Figure 2**). However, a negative effect on biofilm formation was observed.

Characterisation of the role of AcrB substitutions in resistance

To confirm the changes observed within AcrB were responsible for the decreases in susceptibility observed for the corresponding selective drugs we recreated the relevant genotypes in the parent *Salmonella* strain. We then determined their impact on sensitivity to a panel of drugs and on cellular permeability to the efflux substrate, resazurin.

We generated a mutant of the parent strain 14028S lacking *acrB* and complemented it with either wild-type or mutant alleles on a plasmid to determine impacts on

phenotypes observed (**Table 1a**). Introduction of AcrB R717L to the *ΔacrB* background led to resistance against azithromycin only, matching the phenotype of the adapted strains carrying the AcrB R717L mutation. The additional introduction of RamR T18P led not only to a further increase in MIC of azithromycin, but also to MICs to chloramphenicol, nalidixic acid and tetracycline, showing that this substitution does not compromise other substrates and that the overexpression of the efflux pump is the major determinant for MDR (**Table 1a**).

While the complementation of the *acrB* deletion strain with *acrB*-Q176K did not have a detectable impact on cefotaxime resistance (Table 1, b), the complementation of *acrB* in a Δ*acrB*/Δ*ramR* background (which results in overexpression of *acrB* due to loss of RamR, and hence make the impact of the complementation clearer) with the *acrB*-Q176K allele did replicate the phenotype of strains derived from the evolution experiments. Similarly, a strain with chromosomal mutations conferring both AcrB Q176K and EnvZ R397H also showed an MIC of cefotaxime fourfold higher than the parent strain. These data confirmed the specific role of AcrB Q176K in cefotaxime sensitivity, but also showed that a significant change in MIC requires synergistic mutations in either *ramR* or *envZ*.

Impact of substitutions on efflux substrate accumulation and gene expression

To further confirm whether the Q176K and R717L AcrB substitutions altered general drug accumulation or efflux activity, we monitored intracellular accumulation of resazurin [43] (**Figure 2**). Resazurin is a non-fluorescent dye which upon cell-entry undergoes a redox reaction leading to colour change. We used WT (14028S) as our reference and a *tolC* deficient mutant as a control lacking functional efflux. The R717L mutant alone did not show any changes in resazurin accumulation compared to the WT, suggesting the substitution does not impact export of this substrate (**Figure 2a**).

The AcrB Q176K substitution was always present in strains already carrying the EnvZ R397H substitution. We measured resazurin accumulation in strains carrying only the EnvZ substitution, and strains also carrying the additional AcrB Q176K substitution. Mutants carrying EnvZ R397H alone accumulated less resazurin compared to the WT and addition of the AcrB Q176K substitution resulted in further decrease of resazurin accumulation, consistent with an increase in efflux efficiency (**Figure 2b**).

To further confirm the role of the RamR substitution seen under azithromycin exposure on pump expression, we extracted RNA from 48-hour old biofilms, and we measured expression of *acrB* and *ramA* by qRT-PCR, using *gyrB* expression as our internal reference (**Figure 2c**). Both genes were found to be derepressed in the mutants compared to the parent strain.

In silico modelling reveals a distinct role of R717L substitution in substrate specificity of the pump.

Analysis of the 3D structure of *Salmonella* Typhimurium AcrB (*S*TmAcrB) [44], indicated that both the acquired substitutions map within the multisite drug-binding pockets of the transporter, with R717L occupying the front end of the PBP, close to the exit of the substrate channel CH2, and Q176K being located in the DBP (**Figure 3**), suggesting that they may impact drug interaction directly and specifically, rather than having a general or allosteric effect. To gain further mechanistic insight on their effect, we performed *in silico* docking of the respective antibiotics to both WT and mutationally-modified drug binding pockets of *S*TmAcrB.

To enable docking we needed to identify suitable docking templates, based on both the ligand occupancy and functional state of the transporter. The only available experimental structure of *S*TmAcrB (PDB ID: 6Z12) [44], is an apo-structure derived from cryo-electron microscopy at a modest resolution (4.6 Å), making accurate side chain predictions within the respective binding pockets unreliable. Furthermore, the structure is C3-symmetrised, and hence binding pockets could not be assigned to either of the physiologically relevant L, T or O-conformations, making that structure poorly suited for the intended docking studies. Fortuitously, the multisite drug binding pockets of *Salmonella* and *E. coli* AcrB are highly conserved, with only 3 substitutions, namely S48T, E280K and M573L, affecting the lining of the drug-binding pockets. Of these, only M573 is predicted to participate in the binding of macrolide and rifampin-like compounds within the PBP according to the available crystal structures [19,22], while E280K (which is only participating in the formation of the pocket via its main-chain atoms), and the conservative S48T substitution, might have a limited effect in the DBP [19,21]. Taking these considerations into account and following previous protocol [45], we performed ensemble docking of azithromycin and cefotaxime onto the DBP, PBP and CH2 entrance channel (that is, the sites containing the mutated residues) of several homology models of the *Salmonella* AcrB derived from the available high-resolution X-ray crystal structures of the *E. coli*

orthologue, which present the functionally relevant ligand-bound L- and T-conformers [19,46] (see *Methods* for details). For each ligand and each binding site, the top docking pose was further relaxed, as this has been shown to improve accuracy [47].

We first focused our attention on the R717L substitution and performed ensemble docking of azithromycin (abbreviated to Azi below). We performed two separate runs, one centred at the PBP, and the second centred at the CH2 access channel of AcrB. When centring the docking grid on CH2, the top poses in the WT cluster closely together (**Supplementary Figure 3**), and overlap with the site that is involved in substrate binding observed in the L-protomer rifampicin/3-formylrifampicin SV-bound structures [19,22], but not macrolide bound structures. Intriguingly, the top WT docking pose for Azi shows direct involvement of R717 (alongside neighbouring residues N719, L828 and Q830) in ligand coordination (**Figure 4A**), which is consistent with residue contacts seen in rifampicin/3-formylrifampicin SV/rifabutin, but not macrolide-occupied crystal structures.

In the case of the R717L mutant, the poses also cluster tightly together, however they center closer to the front end of the PBP, overlapping the CH2 exit (**Supplementary Figure 3**). Correspondingly, the R717L mutation resulted in radically different coordination of Azi from the one observed in the WT (**Figure 4B**), and loses contact not only with the R717L itself, but also its polar contacts with D681, N719, E826. While Q830 is still providing coordination, several hydrophobic contacts are created from the opposite side of the pocket, notably F664, F666 and P669.

Supporting the idea that the preferred CH2 binding site of Azi diverges in the R717L mutant when compared to the WT, the top pose of binding of Azi to CH2 in the mutant R717L structure has significantly lower binding score (~ 2kcal/mol, **Table 2**), than in the WT protein.

These different affinities can be rationalized by a change of coordination, as while in the R717L-pocket the top pose includes additional coordination with participation of Q830 and retains L728, it loses the essential N719, E826 and L717 contacts. Taken together this suggests that azithromycin features different binding modes to the WT and R717L, with more stable contacts with CH2 in the WT form, which may translate into lower residence times for it in the case of R717L.

After entry via CH2, Azi is thought to move into the PBP, where its primary binding site is located, as demonstrated by several macrolide-AcrB structures [19,22,48]. In agreement with that, when docked at the centre of the PBP (**Figure 4 C,D**), Azi preferentially clusters into the back of this site in both WT and R717L structures. These Azi docking positions broadly overlap with the observed substrate position in the erythromycin-occupied experimental structures [19,22,48], and notably are associated with loss of contact with R/L717. The pseudo binding free energies of the top poses of this compound to the PBP are very similar in both the WT and R717L variants of AcrB (**Table 2**), consistent with our interpretation that the enhanced efflux of Azi seen in the R717L mutant is due to changes in CH2 rather than altered coordination within the PBP itself.

Our docking results suggested that the R717L substitution would mostly impact substrates relying on PBP sequestering, and entering the PBP via CH2 (e.g. macrolides, rifamycins and other ansamycins). Anthracyclines such as doxorubicin and tetracycline antibiotics are also thought to utilise CH2, but appear to bypass PBP altogether and are instead sequestered directly in the DBP [22,46,49], so R717L would be expected to have smaller impact on their efflux. Finally, substrates that enter the PBP via the membrane-linked CH1 (including linezolid, fusidic acid, and novobiocin), and planar cations such as EtBr that are thought to enter directly into DBP via CH3 [22,26], are expected to be relatively unaffected by the R717L. To challenge these predictions, the susceptibility of defined mutants to members of the above compound classes was tested. Consistent with our hypothesis, the MICs of the other tested macrolides and rifampicin were similarly affected, while tetracycline, doxorubicin and novobiocin showed no significant differences, and linezolid was unaffected by the R717L substitution (**Table 3**).

To extend these observations beyond Azi, we conducted additional single-structure docking using AutoDock Vina, using structures PDB 3AOC and 3AOB. The preferential binding mode for most tested compounds appears to be within the back part of the PBP, which consistent with our predictions, appears to be undisturbed by the mutation. The only notable exceptions are for Cla and Ery, which appear to form novel hydrophobic interactions in the front part of the PBP, in the case of R717L. That also coincides with a loss of interaction of these compounds with the R717 side chain and might help explain the observed differences in the MIC (data not shown).

In silico modelling predicts AcrB Q176K affects substrate recognition in a distinct manner to R717L

To investigate the impact of the Q176K substitution on the *S*TmAcrB structure and substrate binding, we performed *in silico* modelling of the distal binding pocket of the *S*TmAcrB using homology models of the *Salmonella* DBP based on the experimental *E. coli* structures, followed by ensemble docking of cefotaxime (Cef) as described above for the PBP (**Supplementary Figure 4**).

The best poses found for Cef in the DBP of the T monomer (after structural relaxation) are shown in **Figure 5**. The corresponding observed binding score is -8.4 and -9.7 kcal/mol for the WT and Q176K, respectively, which is opposite to the situation observed with R717L and Azi binding to the CH2. Here, the introduction of the Lys-residue into the DBP results in a direct increase of hydrogen bonds between the protein and the ligand (**Figure 5B**), which translates into a better fit for the drug and correspondingly higher energy of binding. This suggests that the mechanism by which the Q176K substitution aids Cef export is radically different from that by which R717L substitution affects Azi efflux.
We corroborated these docking results by additional single-structure docking of the related compounds – cephalothin and nitrocefin, both of which showed very limited displacement, but notable change of coordination with the addition of Q176K (data not shown).

Differential abundance of AcrB substitutions in globally dispersed isolates

To determine whether the mutations selected in this study were biologically permissive and in circulation in the real world, we searched for their presence in EnteroBase which contains over 200,000 *Salmonella* genomes deposited from around the globe [50,51]. Whilst we first reported the AcrB R717L allele in 2019 [52], a search of the deposited strains identified it in 12 *S.* Typhimurium isolates originating from patients, livestock and food in the United Kingdom, United States, Ireland, and Denmark, with the first deposition being in 2003 (**Figure 6**). A recent study also identified substitution at R717 in multiple azithromycin-resistant isolates of *S.* Typhi (R717Q) and Paratyphi A (R717L) from patients in Bangladesh [53]. These findings demonstrate that this substitution has been selected on multiple occasions in

different *Salmonella* serotypes around the world. The Q176 substitution was not identified in the database.

Discussion

Antibiotic resistance is a complex phenomenon, and it has become clear that the physiological state of bacteria has a large impact on resistance. Recent work has focused on how biofilms can evolve resistance and has shown that for some species there are biofilms specific routes to resistance, or that developing resistance can affect biofilm formation itself [39,42,54]. In this study, we identified sub-inhibitory concentrations of two critical antibiotics rapidly selected for substitutions within AcrB as a central mechanism underpinning evolution of resistance of *Salmonella* to both in planktonic and biofilm states. Adaptive mutations of RND pump proteins are being increasingly reported and represent a general frontline mechanism of bacterial response to antibiotic and other environmental stress [34,55,56]. However, there is little current understanding of how the various changes reported act mechanistically and what impacts there may be on the capacity of the pump to export other substrates. In this work, we characterise two substitutions in detail, which allows their mechanisms to be understood and demonstrates two fundamentally different modes of action. The importance of the two mutations in the biology of the cell also appears to differ, which may reflect their relative importance in the real world.

One of the first AcrB-specific mutations to be isolated due to antibiotic treatment in a clinical setting resulted in a G288D substitution in *Salmonella* AcrB [30]. This conferred clinically significant ciprofloxacin resistance isolated from an infection which proved fatal to the patient. Additional M78I and P319L substitutions within AcrB have also been identified in ciprofloxacin resistant isolates of *Salmonella* [34]. Substitutions have also been reported within AcrB which confer resistance in *Klebsiella* [55], as well as in the related CmeB RND transporter in *Campylobacter* [56].

R717 is located on the upper side of the access CH2 exit, and contributes to the formation of the frontal part of the PBP, where it can directly coordinate Rifampicin [19], 3-Formylrifamicn [22] and a number of smaller compounds (e.g. ciprofloxacin [57] and doxorubicin [46] in the L-conformers of *E.coli* AcrB. As revealed by a number of experimental structures, R717 is the focus of a multi-residue network, including the side chain of Q830 and backbone atoms of S715 and L828, involved in coordination

of rifampicin, and 3-Formylrifamicin. While R717 is not seen directly interacting with erythromycin molecules in the PBP of the available structures (e.g. PBD ID 3AOC; [19]), it is within interacting distance of other critically important ligand-coordinating residues such as N719, which can provide direct bonding both with the erythromycin substrate alongside E826 (e.g. PDB ID 4ZJQ [48]).

Thus, substitution of R717 with a hydrophobic, bulky leucine residue could be expected to influence efflux efficiency via a direct change in drug coordination, as well as via secondary effects, due to disruption of the charged residue networks, and general changes in the electrostatics and solvation in the pocket. While short of a direct experimental validation, our ensemble docking results support these predictions. Docking of azithromycin to the CH2 entrance of the WT protein resulted in a tight clustering of high affinity poses in proximity of R717 (**Supplementary Figure 3**), with the top pose making extensive direct contact with the side chain of this amino acid (**Figure 4A**). This coordination is not directly observed in the available erythromycin-bound structures, but is highly compatible with the rifampicin, 3-formyl-rifampicin, and rifabutin-bound structures e.g. PDB IDs 3AOB; 6ZOB; 6ZO9 [19,22], and we propose that such a pose represents a valid transient interaction of the macrolide ligands during their transit from the CH2 channel into the PBP proper. The predicted interaction can also readily explain the observed impact of R717 on MICs of both macrolide and ansamycin antibiotics that we observed (**Table 3**). Consistent with this interpretation is the dramatic change of coordination we observed when docking azithromycin to the R717L pocket, resulting in an unexpected shift, or “slippage” of the preferred azithromycin docking positions down towards the bottom of CH2 (**Supplementary Figure 3**, **figure 4B**). This loss of coordination with several residues participating in the stabilisation of the ligand in the WT translates into a significant difference in the estimated binding energy of azithromycin to the R717L pocket. This observation provides strong evidence for a structural impact on CH2 impacting azithromycin transit. However, we also wanted to explore any possible impact on the second, canonical macrolide binding site, within the PBP. There, the preferred docking poses for both WT and R717L overlap and align with experimental macrolide-bound structures [19,22,48] (**Figure 4 C, D**). This is expected, given that this binding site does not allow a direct contact of the ligand with either R717 or L717 side chain, and correspondingly there is no measurable difference in the pseudo binding free energy of azithromycin to this site (**Table 2**). These data are important,

as they suggest, that while the recognition and energy of binding in the back of PBP is not affected by R717L substitution, the mutation has a dramatic impact on the front of the ligand transport pathway (CH2), associated with the initial stages of macrolide/ansamycin transport. Previously, stepwise transfer of substrates through the efflux duct of AcrB has been suggested by the available substrate-occupied X-ray and cryo-EM structures of AcrB [9,19,46,58], as well as by a number of molecular dynamics simulations [49,59,60] and our *in silico* data strongly support these predictions.

Taken together, our analysis suggests that while the R717L mutation affects access to CH2 by the large macrolide compounds, it doesn't affect the PBP's affinity towards these classes of drugs. This was further supported by the differential impacts that the R717L mutation had on drugs predicted to utilise different substrate channels (**Table 3**). Indeed, the observed 2 kcal/mol differences in binding energies between the WT and R717L in the front of the CH2, but not in the back of the PBP, suggests that the retention time of drugs such as azithromycin, might be lower in the mutant, facilitating the drug transition from the CH2 to the back of the PBP, without impacting recognition in the latter. This is important, as it could explain how this substitution does not result in loss of ability to export other AcrB substrates, and so does not prevent the MDR phenotype observed when R717L was overexpressed.

Subsequent to our first description of R717L [52] a recent study by Zwama and Nishino [61], has provided evidence which indicated steric hindrance and electrostatic effects to be the cause of a change in the relative accessibility of the PBP. This supports the work we report here, and we now significantly expand the scope of that study, by providing quantitative assessment of drug binding, and the specific molecular environment within the binding pockets of the pump, to further understand the molecular mechanisms of this mutation.

The importance of changes at R717 (*Salmonella* AcrB numbering) is further supported by a recent report of mutations in the orthologous Neisserial transporter MtrD, associated with increased azithromycin MICs – namely R714G and K823E substitutions [62,63]. This led the authors to speculate that non-mosaic gonococcal strains bearing both the *mtrR* promoter and amino acid changes at MtrD positions 714 or 823 could translate into clinically significant levels of azithromycin resistance. A follow-up study using a global meta-analysis collection of 4,*852 N. gonorrhoeae* genomes [63], did identify the residue R714 of MtrD as a hotspot for mutations leading

to increased MICs against azithromycin arising in clinical settings. Several alleles of R714 have been reported from clinical isolates, including R714L, as well as R714C and R714H. This supports our identification of R717L in various isolates of *Salmonella* serovars from humans and animals around the world (**Figure 6**), and the emergence and spread in azithromycin resistance in *S.* Typhi and *S.* Paratyphi isolates [53]. The fact we observe this mutation to emerge rapidly and have a strong phenotypic impact on azithromycin susceptibility, which does not compromise the ability of AcrB to export other substrates when over-expressed, may make this a variant with significant benefits and helps understand its emergence.

The Q176 residue forms part of the distal binding pocket of AcrB [9,46], specifically participating in the so-called 'DP_T cave' structure of the pocket as defined by [64]. Due to its central position in the DP_T cave, Q176 has been implicated in direct binding to both substrates and non-substrates [21], (e.g. Doxorubicin, 2DR6.pdb [9]; Rhodamine 6G; [65]), as well as competitive pump inhibitors such as D13-9001 (aka P9D) (PDB ID 3W9H; [18,66]), and pyranopyridine derivatives including MBX3135 (PDB ID 5ENR [65]), but not MBX2319. In addition, several carbapenem antibiotics have been suggested to interact directly with the Q176 based on recent MD analysis [66] including ertapenem and biapenem. Recently, this residue has also been found in proximity to the binding site of levofloxacin (PDB ID 7B8T; [67]), further highlighting its critical role in recognition and coordination of substrates.

Docking of cefotaxime to the WT and Q176K DBP pocket shows the side chain in direct contact with the substrate in both cases (**Figure 5, Supplementary Figure 4**). Importantly, and directly opposite to the effect of the R717L however, the Q176K substitution seems to specifically change the binding efficiency of the DB_T towards cefotaxime, as the introduction of the lysine side chain produces several new strong polar contacts with the ligand, which translates to notably more favourable energy of binding and ligand recognition. A similar mechanism is inferred by the nitrocefin and cephalothin docking.

Importantly, the predicted increase in pseudo binding free energy (~1.4 kcal/mol) as a result of the Q176K substitution is likely to improve recognition while keeping the affinity below an "inhibition threshold", which would convert cefotaxime into a competitive inhibitor of the pump by increasing its residence time within the DBP [68-70], as evidenced by previous studies involving *e.g.* MBX2319 *vs* minocycline binding

[71]. Enhanced fitting within the DBP below the inhibition threshold thus translates into increased probability for allosteric conformational change induced in the TM-region and/or correspondingly increased likelihood of a T- to C (O)-transition of the respective AcrB protomers [4,58,72], resulting in more effective overall transport. Whilst our data show that Q176K had improved recognition of cefotaxime, which translates into decreased susceptibility for strains with this change, the phenotypic impact was only evident in combination with change in *envZ* or *ramR*. These act to either reduce drug entry through porin loss, or through over-expression of *acrB* respectively. Notably, we did not identify the Q176K substitution in isolation, and it was not present in the Enterobase database. We recently characterised the role and fitness impacts of the EnvZ substitutions selected as precursors to the emergence of Q176K, and found that mutation of *envZ* had a cost on biofilm formation, potentially affecting its fitness to survive in the environment and cause disease[42]. Given the likely dependence on mutation within *envZ* for the AcrB Q176K to confer a benefit, and the inability to form good biofilms, it's possible that this combination may occur rarely in nature and hence is not recorded on Enterobase.

This work has shown that using laboratory evolution can efficiently and quickly identify mutations which allow bacteria to resist important antibiotics, furthermore this method also allows epistatic relationships to emerge and be identified. This has allowed us to identify two key changes within AcrB, but also to understand their interactions with other regulators which control cellular permeability and stress responses. Importantly we could also identify the probable hierarchy of selection as we reproducibly saw the same mutations emerging in the same sequences in different lineages – azithromycin resistance emerges via selection of AcrB R717L and first and later is accelerated by gain of loss of function changes within *ramR*. In contrast, for cefotaxime a change in EnvZ is the crucial first step before the Q176K AcrB substitution can exert a significant effect. The use of different conditions can also inform the possible fitness outcomes of different combinations of mutations, and we see different permissive routes to resistance in biofilm and planktonic conditions. This is important, as understanding how resistance that emerges in the laboratory setting can inform selection in the real-world, while our ability to model and predict resistance development is an important tool in understanding AMR.

In summary, the combination of laboratory evolution and analysis of mutants has shown the central importance of AcrB in evolution of resistance to major antibiotics,

but also how these substitutions relate to the wider network of genes within the cell which control envelope permeability and have impacts in different growth conditions. Furthermore, we show that despite similar phenotypic manifestations the two described AcrB substitutions employ strikingly divergent molecular mechanisms, providing new insight into how this crucial bacterial defence system operates and can evolve. Understanding the potential fitness trade-offs and changes in lifestyle that are associated with resistance gain acquired via mutations in AcrB and other efflux pumps might provide value in our continuous fight against antibiotic resistance.

Methods

Experimental evolution model

The experimental evolution model was carried out as described in detail in [42]. Briefly, six independent *Salmonella* lineages (two exposed planktonic lineages and four exposed biofilm lineages) were exposed to 0.06 µg/mL of cefotaxime and 10 µg/mL of azithromycin respectively. The lineages were grown in lysogeny broth (LB) with no salt at 30ºC and were serially transferred every 72 hours for 17 passages. Biofilm lineages were grown on 6mm soda lime glass beads. Cells were recovered from the beads by vortexing, three single-cell colonies from passages 1, 9 and 17 were isolated from populations and were stored in 20% glycerol for subsequent phenotyping.

Antimicrobial susceptibility assays

Minimum inhibition concentrations were determined by the broth microdilution method and the agar dilution method in Mueller-Hinton broth or agar respectively, following EUCAST guidelines [73].

Whole genome Sequencing and analysis

Genomic DNA was normalised to 0.5 ng/µL with 10mM Tris-HCl. 0.9 µL of TD Tagment DNA Buffer (Illumina Catalogue No. 15027866) was mixed with 0.09 µL TDE1, Tagment DNA Enzyme (Illumina Catalogue No. 15027865) and 2.01 µL PCR grade water in a master mix and 3ul added to a chilled 96 well plate. 2 µL of normalised DNA (1ng total) was mixed with the 3 µL of the tagmentation mix and heated to 55 ºC for 10 minutes in a PCR block. A PCR master mix was made up using 4 ul kapa2G buffer, 0.4 µL dNTP's, 0.08 µL Polymerase and 4.52 µL PCR grade water, contained in the Kap2G Robust PCR kit (Sigma Catalogue No. KK5005) per sample and 11 µL added to each well need to be used in a 96-well plate. 2 µL of each P7 and P5 of Nextera XT Index Kit v2 index primers (Illumina Catalogue No. FC-131-2001 to 2004) were added to each well. Finally, the 5 µL Tagmentation mix was added and mixed. The PCR was run with 72 ºC for 3 minutes, 95 ºC for 1 minute, 14 cycles of 95 ºC for 10 seconds, 55 ºC for 20 seconds and 72 ºC for 3 minutes. Following the PCR reaction, the libraries were quantified using the Quant-iT dsDNA Assay Kit, high sensitivity kit (Catalogue No. 10164582) and run on a FLUOstar Optima plate reader. Libraries were pooled following quantification in

equal quantities. The final pool was double-spri size selected between 0.5 and 0.7X bead volumes using KAPA Pure Beads (Roche Catalogue No. 07983298001). The final pool was quantified on a Qubit 3.0 instrument and run on a High Sensitivity D1000 ScreenTape (Agilent Catalogue No. 5067-5579) using the Agilent Tapestation 4200 to calculate the final library pool molarity. The pool was run at a final concentration of 1.8 pM on an Illumina Nextseq500 instrument using a Mid Output Flowcell (NSQ® 500 Mid Output KT v2(300 CYS) Illumina Catalogue FC-404-2003) and 15 pM on an Illumina MiSeq instrument. Illumina recommended denaturation and loading recommendations which included a 1% PhiX spike in (PhiX Control v3 Illumina Catalogue FC-110-3001). To determine SNPs between the parent strain and the de novo assembled *Salmonella* genomes, derived from evolved isolates, Snippy version 3.1 was used (https://github.com/tseemann/snippy). Salmonella enterica serovar Typhimurium 14028S (accession number: CP001363), was used as the reference strain for all analysis as it is fully sequenced and annotated.

Identification of the mutations identified in isolates from EnteroBase

The EnteroBase repository holds and curates *Salmonella* genomes including automated annotation of all submissions and assignment of unique allele tags to annotated genes. To identify the presence of strains carrying specific mutations of interest in the database we downloaded all the *acrB* alleles recorded. We then created a local BLAST database for each and used our mutant allele sequences to query these databases and identify alleles with 100% identity, i.e. with the substitution of interest.

In silico modelling and antibiotic docking

*S*TmAcrB structures for ensemble docking were built as follows: 1) several homology models of the wild type, R717L, and Q176K transporters in an asymmetric LTO state were generated using the software Modeller 10.2 [74,75] and the experimental structures with the following PDB codes as templates: 2DHH, 2DR6, 2DRD, 2GIF, 2HRT, 2J8S, 3AOA, 3AOB, 3AOC, 3AOD, 3NOC, 3NOG, 3W9H, 4DX5, 4DX6, 4DX7, 4U8V, 4U8Y, 4U95, 4U96, 4ZIT, 4ZIV, 4ZJL, 5JMN, 5NC5, 5YIL, 6Q4N, 6Q4O, 6Q4P. Each pair of target and template sequences were aligned using Clustal Omega [76]. Next, 10 homology models were built for each template, using the variable target function method to perform the optimisation. Finally, the model with the highest MOLPDF was selected for the next step. 2) Ensemble docking of Azi and

Cef was performed on three different groups of AcrB structures, each defined for docking the compounds to the CH2 entrance, the PBP and the DBP. The groups of structures were chosen by adapting the protocol introduced in [45]. Namely, the 29 homology model structures selected above were aligned to each of the three sites mentioned above, and the corresponding RMSDs at those sites were calculated for each possible pair, resulting in three symmetric 29 × 29 matrices. From each matrix we kept only the structures that exhibited global RMSD values (calculated for all the heavy atoms defining the corresponding site) larger than 1.0 Å from each other. This allowed to include a limited number of non-redundant structures displaying different conformations at the site of interest, which should improve docking accuracy [77,78]. For pairs with RMSDs values below this threshold, we removed the structure with the lowest resolution from the pool. This resulted in 19 (2DHH, 2DR6, 2GIF, 2J8S, 3AOA, 3AOB, 3AOC, 3NOC, 3NOG, 3W9H, 4DX5, 4DX6, 4DX7, 4U8V, 4ZIT, 4ZJL, 5JMN, 5NC5, 6Q4P), 20 (2DHH, 2DR6, 2GIF, 2J8S, 3AOA, 3AOB, 3AOC, 3NOC, 3NOG, 3W9H, 4DX5, 4DX6, 4DX7, 4U8V, 4ZIT, 4ZJL, 5JMN, 5NC5, 5YIL, 6Q4P), and 11 (3AOB, 2DHH, 2DR6, 2GIF, 2J8S, 3AOA, 3AOC, 3NOC, 3NOG, 3W9H, 5YIL) structures used for docking ligands on the CH2 entrance, PBP and DBP, respectively. The aforementioned sites include, respectively, residues 566, 645, 649, 653, 656, 662, 676, 678, 715, 717, 719, 722, 830 (for CH2); 79, 91, 134, 135, 573, 575, 577, 617, 624, 664, 666, 667, 668, 674, 828 (for PBP); and 46, 89, 128, 130, 134, 136, 139, 176, 177, 178, 179, 180, 273, 274, 276, 277, 327, 573, 610, 612, 615, 617, 620, 628 (for DBP).

Docking was performed using the software GNINA [79], setting the number of output poses to 10 and the remaining parameters but the exhaustiveness (128 vs. a default value of 8) to their default values. The grids were centred onto the geometrical centre of the corresponding docking site. This resulted in grids of volumes 35·25·25 $Å^3$, 30·30·30 $Å^3$, and 30·30·30 $Å^3$ for CH2, PBP, and DBP respectively.

For each ligand and each site, the top docking pose was further relaxed using AMBER20, (https://ambermd.org/AmberMD.php) and rescored with Autodock , using the AutoDock VINA scoring function implemented in GNINA to provide a qualitative estimate of the binding affinities [47].

For single-structure docking, AutoDock VINA was used to dock compounds onto (i) *S*TmAcrB PBP, which models were based on the L-conformers occupied by

Erythromycin (PDB ID: 3AOC chain C) and Rifampicin (PDB ID: 3AOB chain C) [19], modified to account for the M573L species-specific substitution; and (ii) *S*TmAcrB DBP, which models were derived from the T-conformer apo-structure (PDB ID: 2J8S chain B), and occupied by minocycline (PDB ID: 4DX5 chain B) [46], modified to account for the species-specific substitutions S48T, E280K. The grids centres and volumes were the same as the ensemble docking.

Preparation of RNA samples for q-RT PCR

RNA from biofilms was isolated using the SV Total RNA Isolation System kit (Promega). RNA was extracted from strains carrying the AcrB R717L and AcrB R717L/ RamR T18P substitutions. Biofilms of these strains were grown on the surface of lysogeny broth agar with no salt and these were incubated for 72 hours at 30ºC. Cells from each biofilm were prepared for lysis in 100 µL TE containing 50 mg/mL lysozyme and were homogenised by vortexing. RNA was isolated following the Promega kit protocol and was eluted using 100 µL of nuclease-free water. RNA quantification was performed using the Qubit RNA High Sensitivity Assay kit (Q32852).

Quantitative Real-Time PCR (q-RT PCR)

To determine expression levels of *acrB* and *ramA*, we performed q-RT PCR using the Luna Universal One-Step RT-qPCR Kit from NEB (E3005), using the Applied BiosystemsTM 7500 Real-Time PCR system. The primers used for the q-RT PCR are listed in Supplementary Table 1. Efficiency of the primers was calculated by generation of calibration curves for each primer pair on serially diluted DNA samples. The R2 of the calibration curves calibrated was ≥0.98 for all the primer pairs used in this study.

RNA at a final amount of 50-100 ng was added to 10 µL final volume PCR reactions, mixed with 400 nM of each primer. The cycle parameters were as follows: 10 minutes at 55 ºC (reverse transcription step), 1-minute denaturation at 95 ºC and 40 cycles of 10 seconds at 95 ºC and 1 minute at 60 ºC.

For each sample, two technical replicates from two biological replicates each were included (four in total) per reaction. Controls with no reverse transcriptase were also included for each RNA sample to eliminate DNA contamination.

To calculate expression levels, expression fold change was calculated using *gyrB* expression as a reference. The relative expression was determined by calculating the logarithmic base 2 of the difference between *gyrB* gene expression and target gene expression per sample.

Drug accumulation assay

To measure changes in cellular membrane permeability to drugs, we used the resazurin accumulation assay. Strains of interest were grown to early exponential phase (OD: 0.2-0.3) using 1:100 inoculum from an overnight culture. The cells were washed with PBS and normalised for cell density before being mixed with 10 μg /mL of resazurin in 100 μL final volume in round-bottom microtiter plates. Fluorescence was measured at 544nm excitation and 590nm emission in an Omega FLUOstar plate reader. Five biological replicates (with three technical replicates assayed for each) were included per strain and resazurin-only reactions were used as controls. The assays repeated on at least two separate occasions with reproducible results observed each time.

Genetic manipulations

For the gene deletion mutants, we used the λ-red gene doctoring technique as described in [80], 300-400 bp-long homologous regions flanking the genes of interest were cloned into the MCS1 and MCS2 of the pDOC-K vector. The cloned regions include the first and last 10 codons of the gene to be deleted, to avoid pleiotropic effects. For the *acrB* and *ramR* deletions, the upstream homologous regions were cloned EcoRI/ BamHI in MCS1 and the downstream ones as XhoI/ NheI in MCS2 of pDOC-K.

For the complementation of *acrB*, we used the pWKS30/ AcrB plasmid previously described [81], expression of the gene is under the control of the pBAD system and induction was achieved with the use of 0.5% (w/v) arabinose.

For complementation of *ramR*, we used the pDOC-K/ glms vector [82]. Wild-type *ramR* and 'ramR-T18P' alleles were cloned XhoI/ HindIII in pDOC-K/ glms under the control of the gene's native promoter.

Data availability

Whole genome sequencing data that support the findings of this study have been deposited in the Sequence Read Archive with the project number PRJNA529870 (accession numbers: SAMN11288384, SAMN11288382, SAMN11288381, SAMN11288380, SAMN11288379, SAMN11288378, SAMN11288370, SAMN11288368, SAMN11288366, SAMN11288361).

Acknowledgements

ET, and MAW were supported by the BBSRC Institute Strategic Programme Microbes in the Food Chain BB/R012504/1 and its constituent project BBS/E/F/000PR10349. Bioinformatics analyses were performed on CLIMB-computing servers, an infrastructure supported by a grant from the UK Medical Research Council (MR/L015080/1).

Author contributions:

ET designed and performed experiments, analysed data and wrote the paper. JAA performed experiments and analysed data. FP analysed data and wrote the paper. AVV designed methodology, performed docking and analysed data. VNB ran *in silico* structural analysis, analysed data and wrote the paper. MAW designed experiments, analysed data and wrote the paper.

Competing Interests

The authors have no competing interests to declare.

References

1 Martinez, J. L. & Baquero, F. Mutation frequencies and antibiotic resistance. *Antimicrob Agents Chemother* **44**, 1771-1777 (2000). https://doi.org:10.1128/aac.44.7.1771-1777.2000

2 Blair, J. M., Webber, M. A., Baylay, A. J., Ogbolu, D. O. & Piddock, L. J. Molecular mechanisms of antibiotic resistance. *Nat Rev Micro* **13**, 42-51 (2015).

3 Piddock, L. J. Clinically relevant chromosomally encoded multidrug resistance efflux pumps in bacteria. *Clin Microbiol Rev* **19**, 382-402 (2006).

4 Alav, I. *et al.* Structure, Assembly, and Function of Tripartite Efflux and Type 1 Secretion Systems in Gram-Negative Bacteria. *Chem. Rev.* **121**, 5479-5596 (2021). https://doi.org:10.1021/acs.chemrev.1c00055

5 Klenotic, P. A., Moseng, M. A., Morgan, C. E. & Yu, E. W. Structural and Functional Diversity of Resistance-Nodulation-Cell Division Transporters. *Chem. Rev.* **121**, 5378-5416 (2021). https://doi.org:10.1021/acs.chemrev.0c00621

6 Li, X. Z., Plésiat, P. & Nikaido, H. The challenge of efflux-mediated antibiotic resistance in Gram-negative bacteria. *Clin Microbiol Rev* **28**, 337-418 (2015). https://doi.org:10.1128/cmr.00117-14

7 Poole, K. Efflux-mediated antimicrobial resistance. *J Antimicrob Chemother* **56**, 20-51 (2005). https://doi.org:10.1093/jac/dki171

8 Seeger, M. A. *et al.* Structural asymmetry of AcrB trimer suggests a peristaltic pump mechanism. *Science* **313**, 1295-1298 (2006). https://doi.org:10.1126/science.1131542

9 Murakami, S., Nakashima, R., Yamashita, E., Matsumoto, T. & Yamaguchi, A. Crystal structures of a multidrug transporter reveal a functionally rotating mechanism. *Nature* **443**, 173-179 (2006).

10 McNeil, H. E. *et al.* Identification of binding residues between periplasmic adapter protein (PAP) and RND efflux pumps explains PAP-pump promiscuity and roles in antimicrobial resistance. *PLoS pathogens* **15**, e1008101 (2019).

11 Chen, M. *et al.* In situ structure of the AcrAB-TolC efflux pump at subnanometer resolution. *Structure* **30**, 107-113.e103 (2022). https://doi.org:10.1016/j.str.2021.08.008

12 Kobayashi, N., Tamura, N., van Veen, H. W., Yamaguchi, A. & Murakami, S. β-Lactam selectivity of multidrug transporters AcrB and AcrD resides in the proximal binding pocket. *The Journal of biological chemistry* **289**, 10680-10690 (2014). https://doi.org:10.1074/jbc.M114.547794

13 Hobbs, E. C., Yin, X., Paul, B. J., Astarita, J. L. & Storz, G. Conserved small protein associates with the multidrug efflux pump AcrB and differentially affects antibiotic resistance. *Proceedings of the National Academy of Sciences of the United States of America* **109**, 16696-16701 (2012). https://doi.org:10.1073/pnas.1210093109

14 Bohnert, J. A. *et al.* Site-directed mutagenesis reveals putative substrate binding residues in the Escherichia coli RND efflux pump AcrB. *J Bacteriol* **190**, 8225-8229 (2008). https://doi.org:10.1128/jb.00912-08

15 Nishino, K. & Yamaguchi, A. Analysis of a complete library of putative drug transporter genes in Escherichia coli. *J Bacteriol* **183**, 5803-5812 (2001). https://doi.org:10.1128/jb.183.20.5803-5812.2001

16 Sulavik, M. C. *et al.* Antibiotic susceptibility profiles of Escherichia coli strains lacking multidrug efflux pump genes. *Antimicrob Agents Chemother* **45**, 1126-1136 (2001). https://doi.org:10.1128/aac.45.4.1126-1136.2001

17 Tsukagoshi, N. & Aono, R. Entry into and release of solvents by Escherichia coli in an organic-aqueous two-liquid-phase system and substrate specificity of the AcrAB-TolC solvent-extruding pump. *J Bacteriol* **182**, 4803-4810 (2000). https://doi.org:10.1128/jb.182.17.4803-4810.2000

18 Nakashima, R. *et al.* Structural basis for the inhibition of bacterial multidrug exporters. *Nature* **500**, 102-106 (2013). https://doi.org:10.1038/nature12300

http://www.nature.com/nature/journal/v500/n7460/abs/nature12300.html#supplementary-information

19 Nakashima, R., Sakurai, K., Yamasaki, S., Nishino, K. & Yamaguchi, A. Structures of the multidrug exporter AcrB reveal a proximal multisite drug-binding pocket. *Nature* **480**, 565-569 (2011).

20 Ruggerone, P., Murakami, S., Pos, K. M. & Vargiu, A. V. RND Efflux Pumps: Structural Information Translated into Function and Inhibition Mechanisms. *Current topics in medicinal chemistry* **13**, 3079-3100 (2013).

21 Vargiu, A. V. & Nikaido, H. Multidrug binding properties of the AcrB efflux pump characterized by molecular dynamics simulations. *Proceedings of the National Academy of Sciences* **109**, 20637-20642 (2012). https://doi.org:10.1073/pnas.1218348109

22 Tam, H. K. *et al.* Allosteric drug transport mechanism of multidrug transporter AcrB. *Nat Commun* **12**, 3889 (2021). https://doi.org:10.1038/s41467-021-24151-3

23 Alav, I., Bavro, V. N. & Blair, J. M. A. A role for the periplasmic adaptor protein AcrA in vetting substrate access to the RND efflux transporter AcrB. *Sci. Rep.* **12**, 4752 (2022). https://doi.org:10.1038/s41598-022-08903-9

24 Schuster, S., Vavra, M. & Kern, W. V. Evidence of a Substrate-Discriminating Entrance Channel in the Lower Porter Domain of the Multidrug Resistance Efflux Pump AcrB. *Antimicrob Agents Chemother* **60**, 4315-4323 (2016). https://doi.org:10.1128/aac.00314-16

25 Tam, H. K. *et al.* Binding and Transport of Carboxylated Drugs by the Multidrug Transporter AcrB. *Journal of molecular biology* **432**, 861-877 (2020). https://doi.org:10.1016/j.jmb.2019.12.025

26 Zwama, M. *et al.* Multiple entry pathways within the efflux transporter AcrB contribute to multidrug recognition. *Nat Commun* **9**, 124 (2018). https://doi.org:10.1038/s41467-017-02493-1

27 Kapach, G. *et al.* Loss of the Periplasmic Chaperone Skp and Mutations in the Efflux Pump AcrAB-TolC Play a Role in Acquired Resistance to Antimicrobial Peptides in Salmonella typhimurium. *Front Microbiol* **11**, 189 (2020). https://doi.org:10.3389/fmicb.2020.00189

28 Grimsey, E. M., Weston, N., Ricci, V., Stone, J. W. & Piddock, L. J. V. Overexpression of RamA, Which Regulates Production of the Multidrug Resistance Efflux Pump AcrAB-TolC, Increases Mutation Rate and Influences Drug Resistance Phenotype. *Antimicrob Agents Chemother* **64** (2020). https://doi.org:10.1128/aac.02460-19

29 Piddock, L. J. V. Clinically relevant chromosomally encoded multidrug resistance efflux pumps in bacteria. *Clinical microbiology reviews* **19**, 382-402 (2006). https://doi.org:10.1128/cmr.19.2.382-402.2006

30 Blair, J. M. *et al.* AcrB drug-binding pocket substitution confers clinically relevant resistance and altered substrate specificity. *Proceedings of the National Academy of Sciences of the United States of America* **112**, 3511-3516 (2015). https://doi.org:10.1073/pnas.1419939112

31 Zwama, M. & Nishino, K. Ever-Adapting RND Efflux Pumps in Gram-Negative Multidrug-Resistant Pathogens: A Race against Time. *Antibiotics (Basel)* **10** (2021). https://doi.org:10.3390/antibiotics10070774

32 Kobylka, J., Kuth, M. S., Müller, R. T., Geertsma, E. R. & Pos, K. M. AcrB: a mean, keen, drug efflux machine. *Ann. N. Y. Acad. Sci.* **1459**, 38-68 (2020). https://doi.org:10.1111/nyas.14239

33 Li, X. Z. & Nikaido, H. Efflux-mediated drug resistance in bacteria: an update. *Drugs* **69**, 1555-1623 (2009). https://doi.org:10.2165/11317030-000000000-00000

34 Yang, L. *et al.* Emergence of two AcrB substitutions conferring multidrug resistance to Salmonella spp. *Antimicrob Agents Chemother* **65** (2021). https://doi.org:10.1128/aac.01589-20

35 Andersson, D. I. & Hughes, D. Antibiotic resistance and its cost: is it possible to reverse resistance? *Nat Rev Microbiol* **8**, 260-271 (2010). https://doi.org:nrmicro2319 [pii]

10.1038/nrmicro2319

36 Alav, I., Sutton, J. M. & Rahman, K. M. Role of bacterial efflux pumps in biofilm formation. *J Antimicrob Chemother* **73**, 2003-2020 (2018). https://doi.org:10.1093/jac/dky042

37 Piddock, L. J. Multidrug-resistance efflux pumps - not just for resistance. *Nat Rev Microbiol* **4**, 629-636 (2006).

38 Costerton, J. W. *et al.* Bacterial biofilms in nature and disease. *Annu Rev Microbiol* **41**, 435-464 (1987). https://doi.org:10.1146/annurev.mi.41.100187.002251

39 Trampari, E. *et al.* Exposure of Salmonella biofilms to antibiotic concentrations rapidly selects resistance with collateral tradeoffs. *NPJ biofilms and microbiomes* **7**, 1-13 (2021).

40 Baucheron, S. *et al.* Bile-mediated activation of the acrAB and tolC multidrug efflux genes occurs mainly through transcriptional derepression of ramA in Salmonella enterica serovar Typhimurium. *J Antimicrob Chemother* **69**, 2400-2406 (2014). https://doi.org:10.1093/jac/dku140

41 Yamasaki, S. *et al.* The crystal structure of multidrug-resistance regulator RamR with multiple drugs. *Nat Commun* **4** (2013). https://doi.org:10.1038/ncomms3078

42 Trampari, E. *et al.* Cefotaxime Exposure Selects Mutations within the CA-Domain of envZ Which Promote Antibiotic Resistance but Repress Biofilm Formation in Salmonella. *Microbiol Spectr*, e0214521 (2022). https://doi.org:10.1128/spectrum.02145-21

43 Vidal-Aroca, F., Meng, A., Minz, T., Page, M. G. & Dreier, J. Use of resazurin to detect mefloquine as an efflux-pump inhibitor in Pseudomonas aeruginosa and Escherichia coli. *J. Microbiol. Methods* **79**, 232-237 (2009). https://doi.org:10.1016/j.mimet.2009.09.021

44 Johnson, R. M. *et al.* Cryo-EM Structure and Molecular Dynamics Analysis of the Fluoroquinolone Resistant Mutant of the AcrB Transporter from Salmonella. *Microorganisms* **8** (2020). https://doi.org:10.3390/microorganisms8060943

45 Malvacio, I. *et al.* Molecular basis for the different interactions of congeneric substrates with the polyspecific transporter AcrB. *Biochim Biophys Acta Biomembr* **1861**, 1397-1408 (2019). https://doi.org:10.1016/j.bbamem.2019.05.004

46 Eicher, T. *et al.* Transport of drugs by the multidrug transporter AcrB involves an access and a deep binding pocket that are separated by a switch-loop. *Proceedings of the National Academy of Sciences of the United States of America* **109**, 5687-5692 (2012). https://doi.org:10.1073/pnas.1114944109

47 Basciu, A., Koukos, P. I., Malloci, G., Bonvin, A. & Vargiu, A. V. Coupling enhanced sampling of the apo-receptor with template-based ligand conformers selection: performance in pose prediction in the D3R Grand Challenge 4. *J. Comput. Aided Mol. Des.* **34**, 149-162 (2020). https://doi.org:10.1007/s10822-019-00244-6

48 Ababou, A. & Koronakis, V. Structures of Gate Loop Variants of the AcrB Drug Efflux Pump Bound by Erythromycin Substrate. *PLoS One* **11**, e0159154 (2016). https://doi.org:10.1371/journal.pone.0159154

49 Zuo, Z., Wang, B., Weng, J. & Wang, W. Stepwise substrate translocation mechanism revealed by free energy calculations of doxorubicin in the multidrug transporter AcrB. *Sci. Rep.* **5**, 13905 (2015). https://doi.org:10.1038/srep13905

50 Achtman, M. *et al.* Genomic diversity of Salmonella enterica -The UoWUCC 10K genomes project. *Wellcome Open Res* **5**, 223 (2020). https://doi.org:10.12688/wellcomeopenres.16291.2

51 Alikhan, N. F., Zhou, Z., Sergeant, M. J. & Achtman, M. A genomic overview of the population structure of Salmonella. *PLoS Genet* **14**, e1007261 (2018). https://doi.org:10.1371/journal.pgen.1007261

52 Trampari, E. *et al.* Antibiotics select for novel pathways of resistance in biofilms. *BioRxiv*, 605212 (2019).

53 Hooda, Y. *et al.* Molecular mechanism of azithromycin resistance among typhoidal Salmonella strains in Bangladesh identified through passive pediatric surveillance. *PLoS Negl. Trop. Dis.* **13**, e0007868 (2019). https://doi.org:10.1371/journal.pntd.0007868

54 Scribner, M. R., Santos-Lopez, A., Marshall, C. W., Deitrick, C. & Cooper, V. S. Parallel Evolution of Tobramycin Resistance across Species and Environments. *mBio* **11** (2020). https://doi.org:10.1128/mBio.00932-20

55 Li, Y., Cross, T. S. & Dörr, T. Analysis of AcrB in Klebsiella pneumoniae reveals natural variants promoting enhanced multidrug resistance. *Res Microbiol* **173**, 103901 (2022). https://doi.org:10.1016/j.resmic.2021.103901

56 Yao, H. *et al.* Emergence of a Potent Multidrug Efflux Pump Variant That Enhances Campylobacter Resistance to Multiple Antibiotics. *mBio* **7** (2016). https://doi.org:10.1128/mBio.01543-16

57 Yu, E. W., Aires, J. R., McDermott, G. & Nikaido, H. A periplasmic drug-binding site of the AcrB multidrug efflux pump: a crystallographic and site-directed mutagenesis study. *J Bacteriol* **187**, 6804-6815 (2005). https://doi.org:10.1128/jb.187.19.6804-6815.2005

58 Eicher, T. *et al.* Coupling of remote alternating-access transport mechanisms for protons and substrates in the multidrug efflux pump AcrB. *Elife* **3** (2014). https://doi.org:10.7554/eLife.03145

59 Reading, E. *et al.* Perturbed structural dynamics underlie inhibition and altered efflux of the multidrug resistance pump AcrB. *Nat Commun* **11**, 5565 (2020). https://doi.org:10.1038/s41467-020-19397-2

60 Vargiu, A. V. *et al.* Water-mediated interactions enable smooth substrate transport in a bacterial efflux pump. *Biochim Biophys Acta Gen Subj* **1862**, 836-845 (2018). https://doi.org:10.1016/j.bbagen.2018.01.010

884 61 Zwama, M. & Nishino, K. Proximal Binding Pocket Arg717 Substitutions in
885 Escherichia coli AcrB Cause Clinically Relevant Divergencies in Resistance Profiles.
886 *Antimicrob Agents Chemother* **66**, e0239221 (2022). https://doi.org:10.1128/aac.02392-21
887 62 Lyu, M. *et al.* Cryo-EM Structures of a Gonococcal Multidrug Efflux Pump Illuminate a
888 Mechanism of Drug Recognition and Resistance. *mBio* **11** (2020).
889 https://doi.org:10.1128/mBio.00996-20
890 63 Ma, K. C., Mortimer, T. D. & Grad, Y. H. Efflux Pump Antibiotic Binding Site
891 Mutations Are Associated with Azithromycin Nonsusceptibility in Clinical Neisseria
892 gonorrhoeae Isolates. *mBio* **11** (2020). https://doi.org:10.1128/mBio.01509-20
893 64 Takatsuka, Y., Chen, C. & Nikaido, H. Mechanism of recognition of compounds of
894 diverse structures by the multidrug efflux pump AcrB of Escherichia coli. *Proceedings of the*
895 *National Academy of Sciences of the United States of America* **107**, 6559-6565 (2010).
896 https://doi.org:10.1073/pnas.1001460107
897 65 Sjuts, H. *et al.* Molecular basis for inhibition of AcrB multidrug efflux pump by novel
898 and powerful pyranopyridine derivatives. *Proceedings of the National Academy of Sciences*
899 *of the United States of America* **113**, 3509-3514 (2016).
900 https://doi.org:10.1073/pnas.1602472113
901 66 Atzori, A. *et al.* Molecular Interactions of Carbapenem Antibiotics with the Multidrug
902 Efflux Transporter AcrB of Escherichia coli. *Int. J. Mol. Sci.* **21** (2020).
903 https://doi.org:10.3390/ijms21030860
904 67 Ornik-Cha, A. *et al.* Structural and functional analysis of the promiscuous AcrB and
905 AdeB efflux pumps suggests different drug binding mechanisms. *Nat Commun* **12**, 6919
906 (2021). https://doi.org:10.1038/s41467-021-27146-2
907 68 Dey, D., Kavanaugh, L. G. & Conn, G. L. Antibiotic Substrate Selectivity of
908 Pseudomonas aeruginosa MexY and MexB Efflux Systems Is Determined by a Goldilocks
909 Affinity. *Antimicrob Agents Chemother* **64** (2020). https://doi.org:10.1128/AAC.00496-20
910 69 Kinana, A. D., Vargiu, A. V. & Nikaido, H. Effect of site-directed mutations in
911 multidrug efflux pump AcrB examined by quantitative efflux assays. *Biochem. Biophys. Res.*
912 *Commun.* **480**, 552-557 (2016). https://doi.org:10.1016/j.bbrc.2016.10.083
913 70 Vargiu, A. V. *et al.* Effect of the F610A Mutation on Substrate Extrusion in the AcrB
914 Transporter: Explanation and Rationale by Molecular Dynamics Simulations. *Journal of the*
915 *American Chemical Society* **133**, 10704-10707 (2011). https://doi.org:10.1021/ja202666x
916 71 Vargiu, A. V., Ruggerone, P., Opperman, T. J., Nguyen, S. T. & Nikaido, H.
917 Molecular mechanism of MBX2319 inhibition of Escherichia coli AcrB multidrug efflux pump
918 and comparison with other inhibitors. *Antimicrob Agents Chemother* **58**, 6224-6234 (2014).
919 https://doi.org:10.1128/aac.03283-14

920 72 Glavier, M. *et al.* Antibiotic export by MexB multidrug efflux transporter is allosterically
921 controlled by a MexA-OprM chaperone-like complex. *Nat Commun* **11**, 4948 (2020).
922 https://doi.org:10.1038/s41467-020-18770-5
923 73 (EUCAST), T. E. c. o. a. s. t. (2016).
924 74 Grimsey, E. M. *et al.* Chlorpromazine and Amitriptyline Are Substrates and Inhibitors
925 of the AcrB Multidrug Efflux Pump. *mBio* **11** (2020). https://doi.org:10.1128/mBio.00465-20
926 75 Webb, B. & Sali, A. Comparative Protein Structure Modeling Using MODELLER. *Curr*
927 *Protoc Bioinformatics* **54**, 5 6 1-5 6 37 (2016). https://doi.org:10.1002/cpbi.3
928 76 Sievers, F. *et al.* Fast, scalable generation of high-quality protein multiple sequence
929 alignments using Clustal Omega. *Mol Syst Biol* **7**, 539 (2011).
930 https://doi.org:10.1038/msb.2011.75
931 77 Asthana, S., Shukla, S., Ruggerone, P. & Vargiu, A. V. Molecular mechanism of viral
932 resistance to a potent non-nucleoside inhibitor unveiled by molecular simulations.
933 *Biochemistry* **53**, 6941-6953 (2014). https://doi.org:10.1021/bi500490z
934 78 Basciu, A., Malloci, G., Pietrucci, F., Bonvin, A. & Vargiu, A. V. Holo-like and
935 Druggable Protein Conformations from Enhanced Sampling of Binding Pocket Volume and
936 Shape. *J. Chem. Inf. Model.* **59**, 1515-1528 (2019). https://doi.org:10.1021/acs.jcim.8b00730
937 79 McNutt, A. T. *et al.* GNINA 1.0: molecular docking with deep learning. *J. Cheminform.*
938 **13**, 43 (2021). https://doi.org:10.1186/s13321-021-00522-2
939 80 Lee, D. J. *et al.* Gene doctoring: a method for recombineering in laboratory and
940 pathogenic Escherichia coli strains. *BMC Microbiol* **9**, 252 (2009).
941 https://doi.org:10.1186/1471-2180-9-252
942 81 Baugh, S., Ekanayaka, A. S., Piddock, L. J. & Webber, M. A. Loss of or inhibition of
943 all multidrug resistance efflux pumps of Salmonella enterica serovar Typhimurium results in
944 impaired ability to form a biofilm. *J Antimicrob Chemother* **67**, 2409-2417 (2012).
945 https://doi.org:10.1093/jac/dks228
946 82 Holden, E. R., Wickham, G. J., Webber, M. A., Thomson, N. M. & Trampari, E. Donor
947 plasmids for phenotypically neutral chromosomal gene insertions in Enterobacteriaceae.
948 *Microbiology* **166**, 1115-1120 (2020).

949

950

Figure Legends

Figure 1: Selection of substitutions within AcrB in different conditions. A. Azithromycin selection. Three isolates were phenotyped and sequenced from biofilms passaged 1, 9, and 17 times, respectively. AcrB R717L emerged after passage 1 and led to an 8-fold increase in azithromycin MIC. Five isolates (out of the 6) from passages 9 and 17 also carried an additional RamR T18P substitution conferring a 4-fold additional increase in azithromycin MIC. **B.** Cefotaxime selection. Three isolates from a planktonic population were phenotyped and sequenced after passages 1, 9, and 17. Mutations within *envZ* emerged after passage 1 conferring 4-fold increase in MIC. By passage 9, the AcrB Q176K substitution emerged, which led to a 16-fold change in MIC. Isolates from passage 17 exhibited a 4-8-fold change in MIC. Any MIC change of 2-fold or above was considered significant. Long horizontal bars indicate the average value for each condition and smaller error bars the standard deviation.

Figure 2. Accumulation of the efflux substrate resazurin and expression of efflux genes. **A,** Reduced accumulation was observed in strains carrying both AcrB R717L and RamR T18P substitutions ($p < 0.0001$) **B, Mutants carrying EnvZR397H exhibited decreased drug accumulation.** Additional mutation within AcrB (Q176K), led to a greater reduction in accumulation of resazurin in the cells ($p < 0.0001$). *tolC::cat*, pump-defective mutant, was used as a control. **C, qRT-PCR in 48-hour biofilms**. Expression of *acrB* and *ramA* was monitored in an isolate carrying the AcrB R717L substitution and in a strain carrying both the AcrB R717L and the additional RamR T18P. Increase of expression of *acrB* and *ramA* was significantly higher compared to the WT in the presence of the RamR T18P substitution. Error bars reflect estimates +/- one standard error. Statistical significance was calculated using a two-way Anova test.

Figure 3. Structural organization of the AcrB trimer indicating the location of mutated residues with relevant substitutions and their relation to the proximal and distal binding pockets. A single protomer (protomer 2) is annotated, with transmembrane helices and the funnel domain in dark grey, while the porter domain sub-domains

(PN1, PC1, PN2 and PC2), which form the main substrate recognition channels and drug binding pockets colour coded. Approximate locations of the PBP and DBP are given with dotted circles. The sidechains of R717 and Q176 are shown as sticks. The switch loop, separating the PBP from DBP is coloured in orange, and the conserved residues F615 and F617, which belong to the loop are also shown as sticks for reference. Illustration based on the experimental structure of the *S*TmAcrB 6Z12.PDB [44].

Figure 4. Docking of Azithromycin to the entrance of CH2 and PBP. All residues within 2.5 Å of the docked ligands (plus the residue R/L717) are shown in stick representation. **A**. Relaxed top pose of azithromycin bound to the entrance of CH2 in the WT, showing ligand coordination with the participation of R717 (purple thick sticks). Dotted lines represent polar contacts. Additional charged (red) and polar (green) residues providing essential contacts are T676, D681, N719 and Q830, as well as the hydrophobic F664, L828 and M862 (in orange). **B.** The CH2 entrance in the R717L variant, showing radically different coordination of the ligand, as it slips towards CH2 losing contact with L717(purple) and forming new contacts in opposite side of the channel – e.g. F666 and P669. **C.** Relaxed top pose for azithromycin bound to the PBP. The R717 does not participate in coordination of the azithromycin. Note the participation of E826 and the gating-loop residues F617 and A618 in coordination. **D.** Relaxed top pose for azithromycin bound to the R717L PBP, showing minor adjustment of coordination, with participation of the gating loop and involvement of Q89.

Figure 5. Effect of Q176 substitution on the coordination of cefotaxime in the deep binding pocket from ensemble docking studies. A. Relaxed top pose coordination showing the essential residues in the WT. Side chain of the Q176 (thick purple sticks) directly participates in ligand binding, providing polar contacts; Ligand binding is additionally supported by predominantly hydrophobic interactions (orange). **B.** Relaxed top pose for Q176K, demonstrating the increased coordination with the participation of K176. S135 and G179 (via main chain) provide additional polar contacts (green), however overall, the position of the Cef in the DBP remains nearly identical to the one observed in the WT.

Figure 6: Identification of R717L in geographically diverse isolates. The map shows where isolates carrying AcrB with the R717L substitution have been reported. Isolates from swine are indicated by purple, clinical isolates with blue, and isolates from the food chain are highlighted green. Isolates of S. Typhimurium were isolated from the United States, United Kingdom, Ireland and Denmark. Clinical isolates of S. Typhi, resistant to azithromycin were recorded in Bangladesh [53]. Isolates carrying the R717L allele were isolated between 2003 and 2019.

a

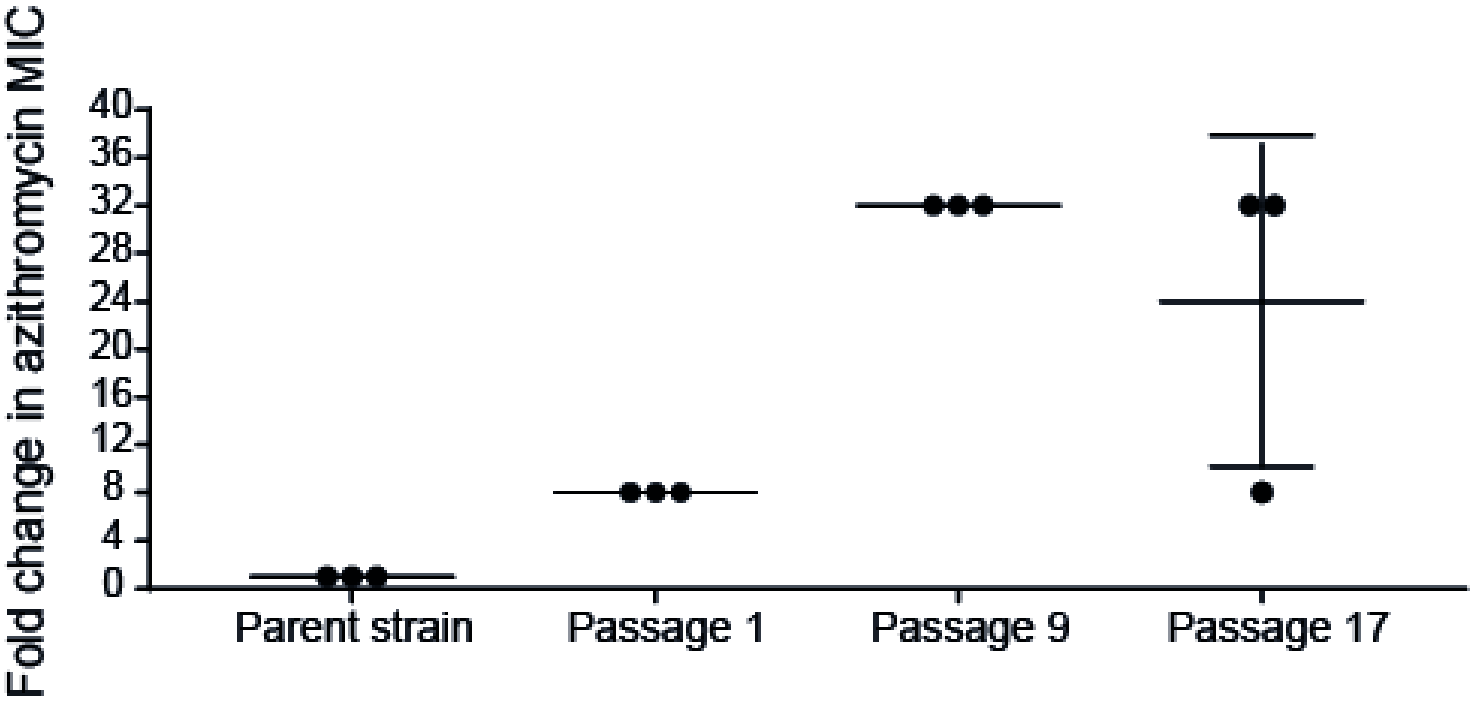

Substitutions

AcrB R717L	X	3/3	3/3	3/3
RamRT18P	X	X	3/3	2/3

b

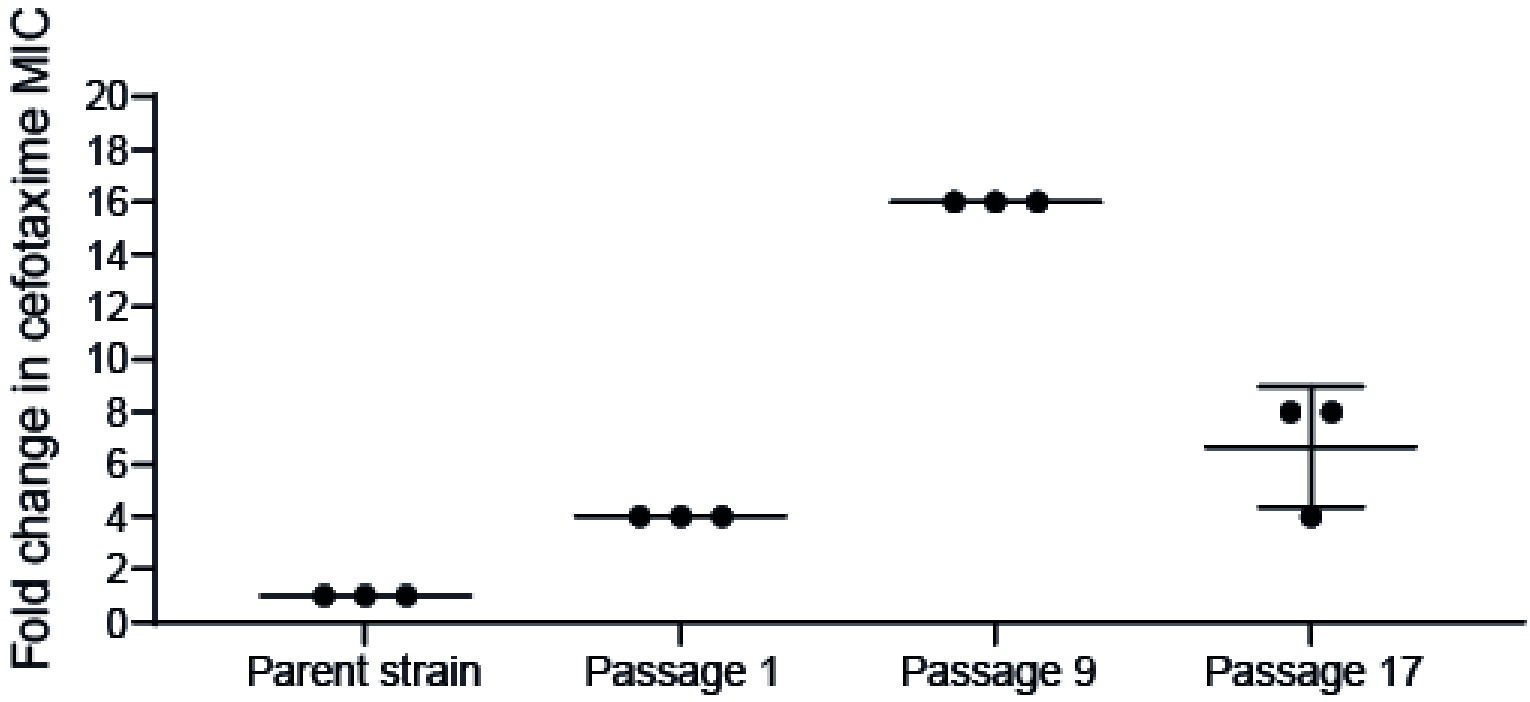

Substitutions

EnvZ	X	3/3	3/3	3/3
AcrB Q176K	X	X	3/3	2/3

Drug accumulation

a

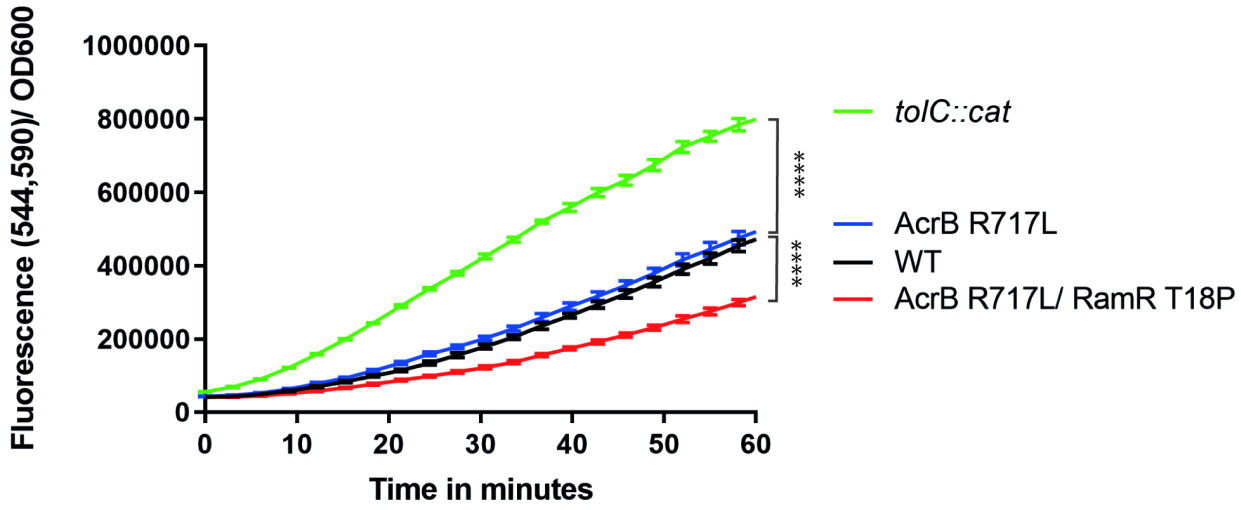

b

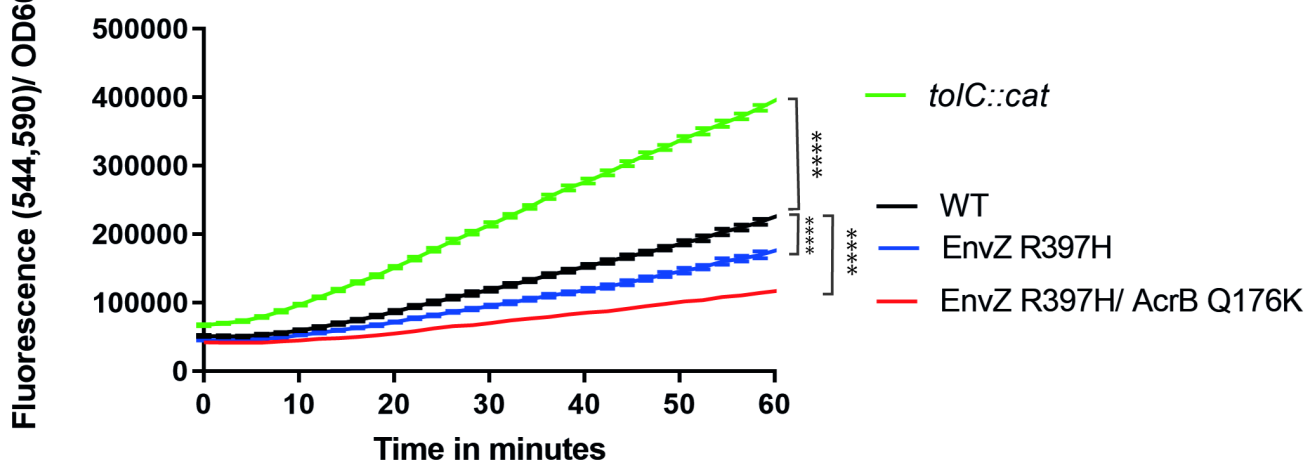

Gene expression

c

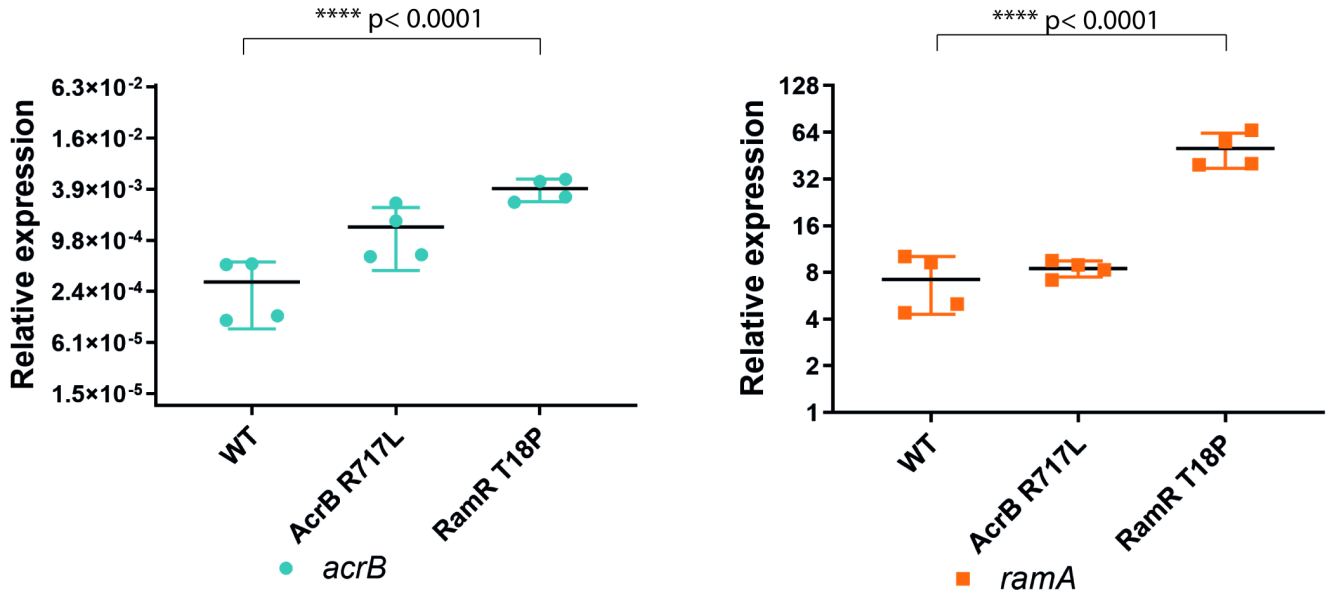

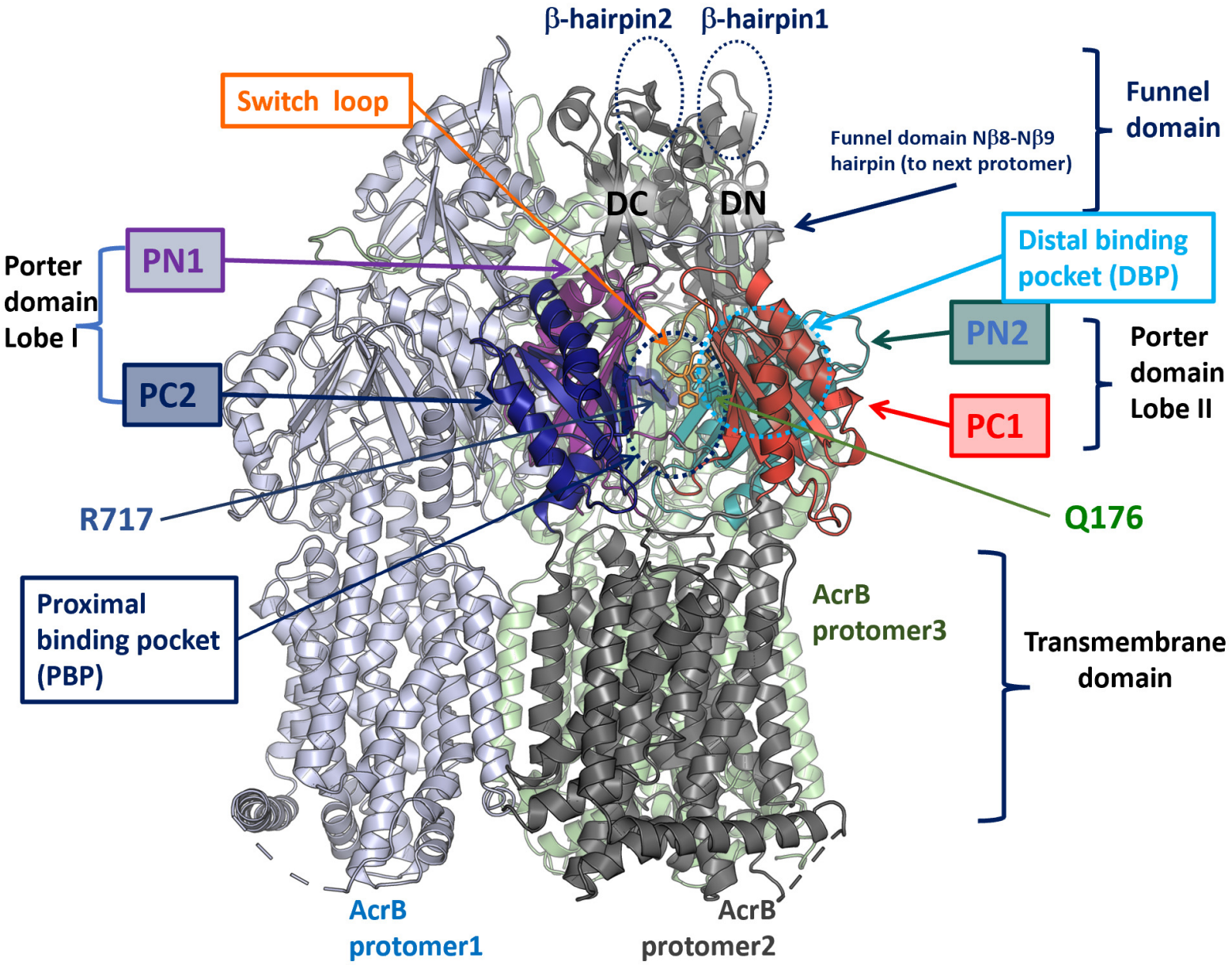
β-hairpin2
β-hairpin1
Switch loop
Funnel domain Nβ8-Nβ9 hairpin (to next protomer)
Funnel domain
DC
DN
Distal binding pocket (DBP)
Porter domain Lobe I
PN1
PC2
PN2
PC1
Porter domain Lobe II
R717
Q176
Proximal binding pocket (PBP)
AcrB protomer3
Transmembrane domain
AcrB protomer1
AcrB protomer2

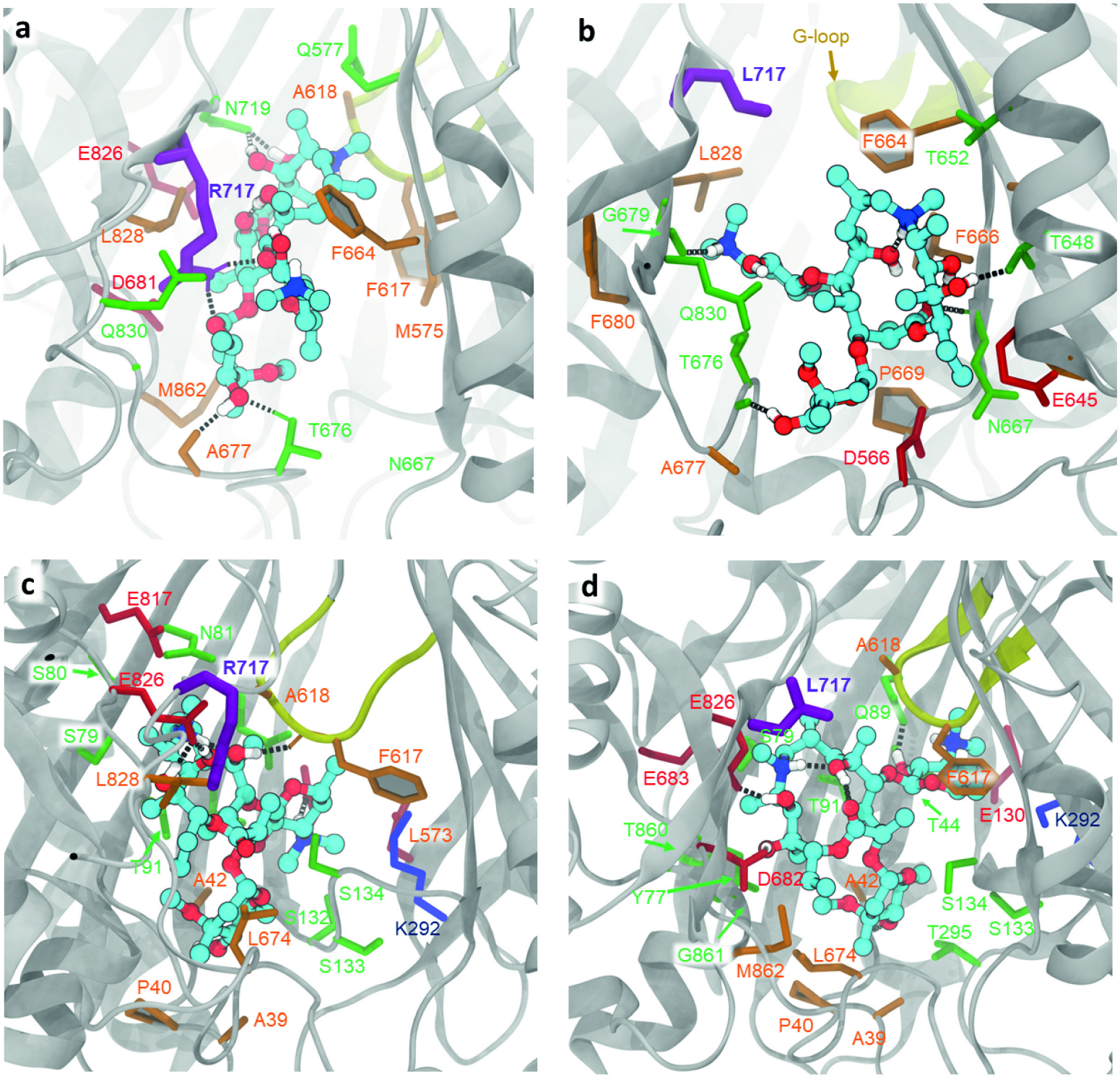
a
Q577
A618
N719
E826
R717
L828
F664
D681
F617
Q830
M575
M862
T676
A677
N667
b
G-loop
L717
L828
F664
T652
G679
F666
T648
F680
Q830
T676
P669
E645
N667
A677
D566
c
E817
N81
S80
E826
R717
A618
S79
F617
L828
L573
T91
A42
S134
S132
K292
L674
S133
P40
A39
d
A618
L717
E826
Q89
S79
E683
F617
T91
T44
E130
K292
T860
D682
A42
Y77
S134
T295
S133
G861
L674
M862
P40
A39

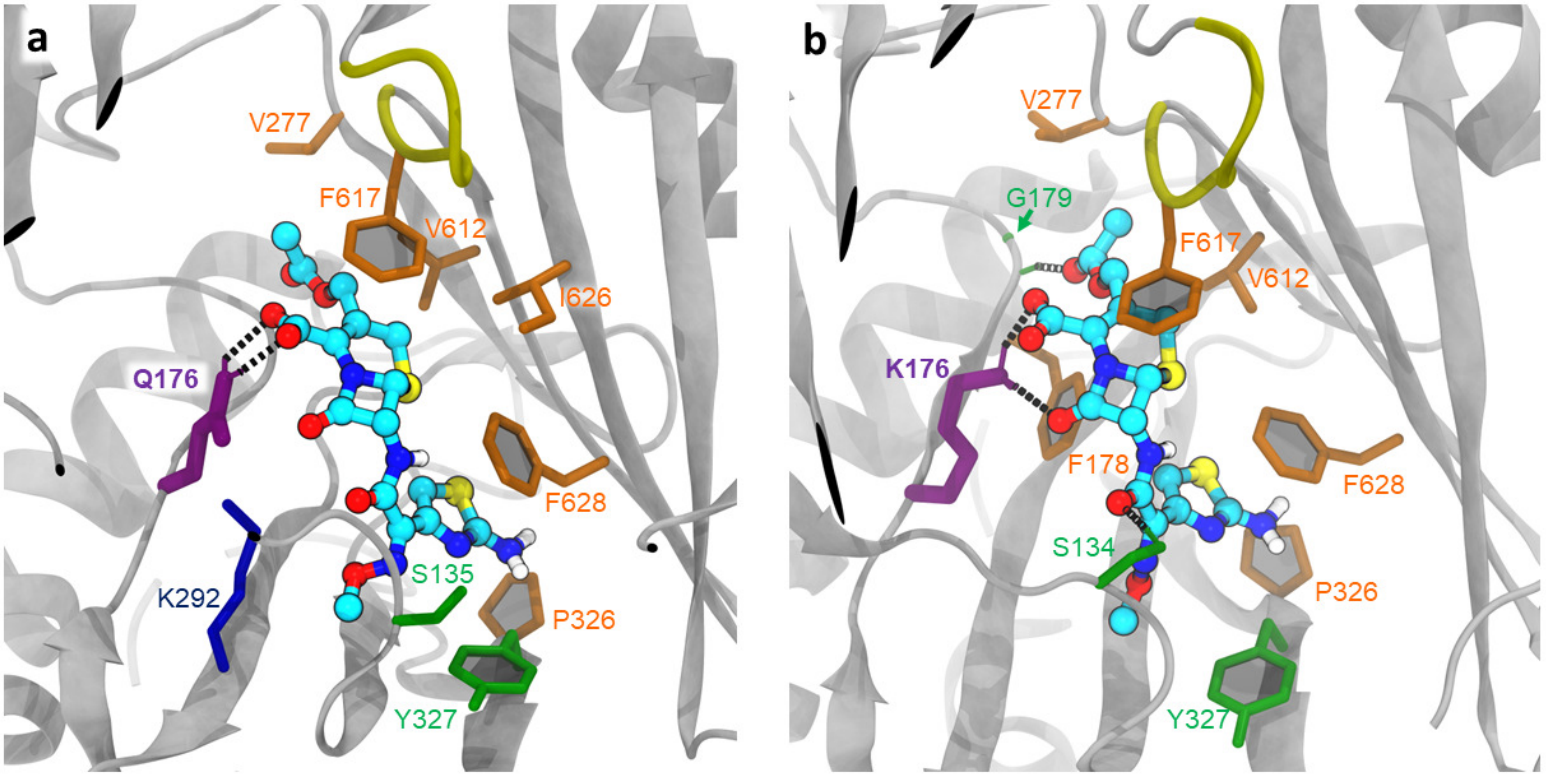
a
V277
F617
V612
I626
Q176
F628
K292
S135
P326
Y327
b
V277
G179
F617
V612
K176
F178
F628
S134
P326
Y327

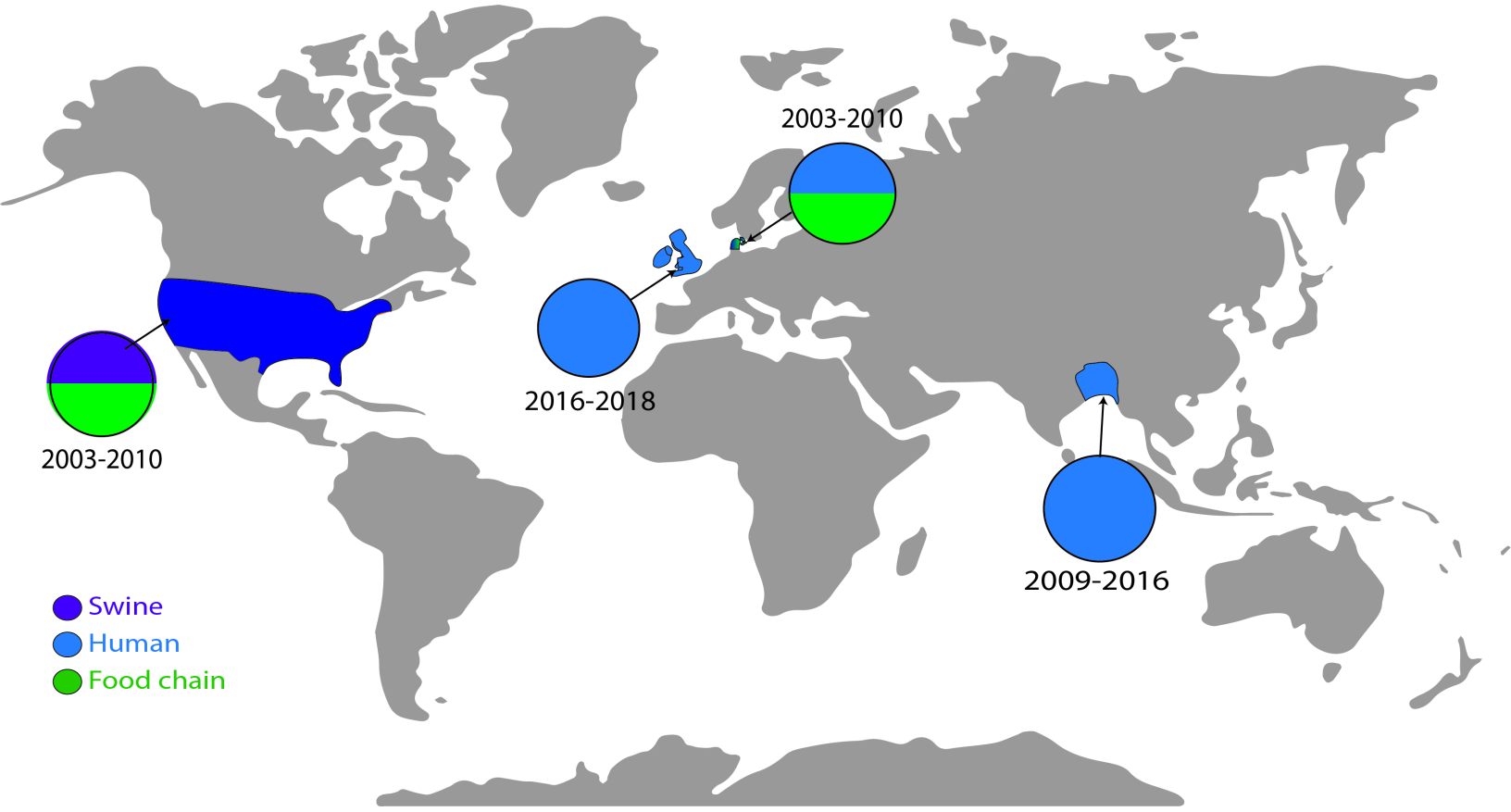
2003-2010
2016-2018
2003-2010
2009-2016
Swine
Human
Food chain

Tables

Table 1: Reconstitution of *acrB* genotypes confirms impacts on susceptibility.

A	**MIC (µg/ml)** **WT**	**AcrB R717L**	**AcrB R717L RamR T18P**	***ΔacrB***	***ΔacrB* p*acrB***	***ΔacrB* p*acrB*_R717L**
Azithromycin	4	**32**	**64**	*0.5*	4	**16**
Cefotaxime	0.125	0.06	0.125	*0.015*	0.125	0.125
Chloramphenicol	4	8	**16**	*0.5*	4	4
Ciprofloxacin	0.03	0.03	0.06	0.03	0.015	0.03
Kanamycin	4	4	2	4	4	4
Nalidixic acid	2	2	**8**	*0.5*	2	2
Tetracycline	0.5	0.5	**2**	*0.125*	0.5	0.5
	ΔramR	***ΔramR* p*ramR***	***ΔramR* p*ramR_T18P***	***ΔacrB,ΔramR***	***ΔacrB,ΔramR* p*acrB***	***ΔacrB,ΔramR* p*acrB_R717L***
Azithromycin	**16**	4	**16**	*0.5*	4	**16**
Cefotaxime	0.25	0.06	0.25	*0.015*	0.25	0.125
Chloramphenicol	**16**	4	**16**	*0.5*	8	8
Ciprofloxacin	0.06	0.03	0.06	0.03	0.03	0.06
Kanamycin	4	ND	ND	2	4	4
Nalidixic acid	**8**	2	**8**	*0.5*	4	4
Tetracycline	**2**	0.5	**2**	*0.125*	1	1

B	**WT**	**EnvZ R397H**	**EnvZ R397H AcrB Q176K**	***ΔenvZ***	***ΔenvZ* p*envZ***	***ΔenvZ* p*envZ_R397H***
Azithromycin	4	4	2	4	4	8
Cefotaxime	0.125	**0.5**	**1**	0.125	0.125	**0.5**
Chloramphenicol	4	**16**	**16**	8	ND	**16**
Ciprofloxacin	0.03	0.06	0.03	0.03	0.03	0.06
Kanamycin	4	2	4	4	ND	ND
Nalidixic acid	2	4	4	2	2	4

Tetracycline	0.5	1	**2**	0.5	0.5	1
	ΔacrB	***ΔacrB* p*acrB***	***ΔacrB* p*acrB_Q176K***	***ΔacrB,ΔramR***	***ΔacrB,ΔramR* p*acrB***	***ΔacrB,ΔramR* p*acrB_Q176K***
Azithromycin	*0.5*	2	2	*0.5*	4	2
Cefotaxime	*0.015*	0.125	0.125	*0.015*	0.25	**1**
Chloramphenicol	*0.5*	4	**8**	*0.5*	8	**16**
Ciprofloxacin	0.03	0.015	0.015	0.03	0.03	0.03
Kanamycin	4	4	4	2	4	4
Nalidixic acid	*0.5*	2	2	*0.5*	4	4
Tetracycline	*0.125*	0.5	1	*0.125*	1	**2**

A. Complementation of AcrB R717L in *ΔacrB* and of RamR T18P in *ΔramR* background reproduced the resistance profiles of the strains isolated from the evolution experiments, confirming that these substitutions are key to the resistant phenotypes observed. **B.** Complementation of Q176K in the *ΔacrB* background had no pronounced impact on cefotaxime resistance until combined with either *ΔramR* or EnvZ R397H, where it then conferred decreased susceptibility to cefotaxime, chloramphenicol, and tetracycline causing an MDR phenotype. ND indicates not determined due to presence of confounding resistance cassettes. Values in bold indicate a fourfold or higher increase in MIC compared to the WT, and those in italics a fourfold or higher decrease.

Table 2. Pseudo-free energy of binding of top poses of azithromycin for the two ensemble docking runs in the CH2 and PBP after relaxation

Top poses from ensemble docking	**Centre on CH2 kcal/mol**	**Centre on PBP kcal/mol**
WT	-11.8	-13.9
R717L	-10.0	-13.9

.

Table 3. **MICs of compounds which do not utilise CH2 are not affected by R717L.**

MIC(µg/ml)	Azi	Ery	Cla	Tet	Rif	Lin	Nov	Dox
14028S (WT)	8	64	64	1	12	256	200	200
14028S ΔAcrB	1	2	2	0.25	6	8	3.125	1.56
ΔAcrB/ pWKS30-pacrB_WT	8	64	32	0.5	6	128	100	200
ΔAcrB/pWKS30-pacrB_R717L	**64**	**256**	**256**	0.5	6	128	50	200

Azi, azithromycin, Ery, erythromycin, Cla, clarithyromycin, Tet, tetracycline, Rif, rifampicin, Lin, linezolid, Nov, novobiocin, Dox, doxorubicin. Results show the mean of three independent experiments. Bold values indicate significant changes.